NASA TECHNICAL NOTE

NASA TN D-2498

c. 1

NASA TN D-2498

WIND-TUNNEL TEST OF A FULL-SCALE, 1.1 PRESSURE RATIO, DUCTED LIFT-CRUISE FAN

by Demo J. Giulianetti, James C. Biggers, and Victor R. Corsiglia

Ames Research Center
Moffett Field, Calif.

NATIONAL AERONAUTICS AND SPACE ADMINISTRATION • WASHINGTON, D. C. • NOVEMBER 1964

WIND-TUNNEL TEST OF A FULL-SCALE, 1.1 PRESSURE RATIO, DUCTED LIFT-CRUISE FAN

By Demo J. Giulianetti, James C. Biggers, and Victor R. Corsiglia

Ames Research Center
Moffett Field, Calif.

NATIONAL AERONAUTICS AND SPACE ADMINISTRATION

For sale by the Office of Technical Services, Department of Commerce, Washington, D.C. 20230 -- Price $1.25

WIND-TUNNEL TEST OF A FULL-SCALE, 1.1 PRESSURE RATIO, DUCTED LIFT-CRUISE FAN

By Demo J. Giulianetti, James C. Biggers, and Victor R. Corsiglia

Ames Research Center
Moffett Field, Calif.

SUMMARY

A fixed blade angle, ducted, tip-turbine-driven fan was investigated as a propulsive cruise device. Results are presented for cruise conditions and transition conditions to high duct angles. Thrust and longitudinal aerodynamic characteristics are shown for various duct exit areas at duct angles ranging from -4° to $+80^{\circ}$ and for forward speeds ranging from 0 to about 180 knots. Duct inlet stall boundaries and representative duct inlet pressure distributions are included.

Increases in lift and positive pitching moment accompanied increases in duct angle. Losses in lift and thrust and reductions of positive pitching moments accompanied duct inlet stall. Inlet flow separation at duct stall was restricted to the lower portions of the inlet. Maximum descent velocities, as limited by duct inlet stall for an airplane assumed to have two ducted lift-cruise fans, varied from approximately 1160 to about 2150 ft/min for various conditions of forward speed, duct angle, and wing loading. Duct exit area variation was effective for maintaining high levels of net thrust with changes in forward speed.

INTRODUCTION

There has been a continually increasing interest in the use of ducted cruise fans as propulsive devices for aircraft in the high subsonic speed range of 0.6 to 0.8 Mach number. The desirability of obtaining large static thrust for V/STOL while still maintaining high subsonic cruise capability led to the design of the tip-turbine-driven cruise fan. Conversion of the high disk loading of a turbojet gas generator to the lower disk loading of the fan results in increases in static thrust for the same power input. Previous tests using the tip-turbine-driven fan of this investigation have shown a static thrust augmentation of 2.8 over that of the plain turbojet used as the gas generator (ref. 1). Subsequent tests (refs. 2 through 5) indicated the feasibility of these fan units as direct lifting devices in wings and fuselages of V/STOL aircraft. The present investigation was made using a tip-turbine-driven fan incorporated into a ducted cruise fan design. Duct exit area was varied in the absence of variable blade angle capability in an attempt to maintain design pressure ratio across the fan with changes in

forward speed. The purposes of this investigation were to study performance and aerodynamic characteristics of the ducted cruise fan as a propulsive device for subsonic cruise flight and to determine its suitability for V/STOL application as a tilting ducted fan during the transition from hover to forward flight.

Tests were conducted at zero and low forward speeds to about 180 knots and for a duct angle range of -4° to $+80^{\circ}$. Three-component longitudinal aerodynamic characteristics were measured. The effect of duct inlet stall on the model characteristics, inlet stall boundaries in descending flight, and representative duct internal pressure distributions upstream of the fan for conditions preceding and following inlet stall were determined.

NOTATION

A_e duct exit area, sq ft

$A_{e,s}$ reference duct exit area, 19.57 sq ft

$\bar{c}$ duct chord, 12.71 ft

C_D drag coefficient, $\frac{D}{Sq_\infty}$

C_L lift coefficient, $\frac{L}{Sq_\infty}$

C_m pitching-moment coefficient, $\frac{M}{S\bar{c}q_\infty}$

D drag, lb

D_f fan diameter, 5.21 ft

L lift, lb

M pitching moment about model moment center, ft-lb

N corrected fan rotational speed, rpm

P_o standard atmospheric pressure, 2116 lb/sq ft

P_s test-section static pressure lb/sq ft

P_T total pressure, lb/sq ft or inches of water

q dynamic pressure, lb/sq ft or inches of water

r inlet radial distance from duct center line at rake station, in. or ft

R	maximum inlet radius at rake station or radius defining duct external contour, in. or ft
S	total projected frontal area, 39.30 sq ft
S_w	reference wing area used for performance calculations, 300 sq ft
T	thrust along fan axis, lb
T_s	reference static thrust at 100-percent fan speed, 7500 lb
V	velocity, ft/sec or knots
V_T	fan tip speed, $\frac{\pi N D_f}{60}$, ft/sec
$\frac{W}{S_w}$	wing loading, $\frac{\text{gross weight}}{300}$, lb/ft^2
X,Y	duct axial and radial coordinates, respectively, in.
α	duct angle, angle of thrust axis to free stream, deg
β	circumferential position from top of duct, deg
δ	relative static pressure, $\frac{P_s}{P_o}$
θ	relative temperature ratio, ambient temperature (absolute)/460°
μ	fan tip speed ratio, $\frac{V_\infty}{V_T}$
ΔP_{loss}	loss in total pressure

Subscripts

l	local
i	inlet
∞	free stream
π	external duct

MODEL DESCRIPTION

Photographs of the model installed in the test section of the Ames 40- by 80-foot wind tunnel are shown in figure 1. Model dimensions and geometry are given in figure 2.

Model Installation

The model was supported by horizontal tubes extending from the duct to the struts on each side of the model. A third support was a pitch-drive mechanism that held the model in position and was used to change duct angle. The pitch-drive mechanism was secured to the top of the right (starboard) strut and consisted of a screw driven by an electric motor through a speed reducer. The entire model support system, including the pitch-drive mechanism, was shielded from the free-stream air by sheet metal fairings which were independent of the model and the wind-tunnel force measuring system.

Duct and Centerbodies

Coordinates defining the duct internal and external contours are given in table I. External duct contour coordinates are listed for circumferential positions around the duct and define the duct shape up to the front face of the fan frame (station 68, fig. 2). The duct inlet lip was relatively thick to favor low forward speed conditions. External duct contours from the front face of the fan frame to the duct trailing edge are defined by radii listed in table I. Centerbody geometry is defined by coordinates listed in table II. Coordinates are given for the inlet centerbody upstream of the fan and for three interchangeable diffuser centerbodies downstream of the fan. An alternate duct trailing edge extended the duct 8 inches and resulted in a smaller duct exit diameter (fig. 2). The three diffuser centerbodies in combination with the two duct exit configurations allowed testing of six exit areas. The largest exit area (area ratio of 1.0) was intended to produce the design pressure ratio across the fixed blade angle fan at zero and low forward speeds. The configuration giving an exit area ratio of 0.62 was intended for a design cruise speed of 0.6 Mach number at 100-percent fan speed. The other configurations were tested to evaluate effects at off-design speed conditions.

Fan and Gas Generator

The fan was a full scale, 1.1 pressure ratio, tip-turbine-driven fan described in references 3 and 4. For this investigation, however, the exit vanes mounted behind the stators were removed. The fan was driven by a turbojet engine enclosed in a nacelle mounted above the duct. The nacelle leading edge extended forward of the duct leading edge as shown in figures 1(a) and 2.

The engine exhaust gases driving the fan were exhausted into the duct downstream of the fan through a shallow annulus section encompassing 173° of azimuth as shown in figure 2.

Pressure Rakes

Internal flow characteristics in the inlet upstream of the fan were measured by pressure rakes located as shown in figure 2. Boundary-layer rakes were mounted on the duct inner walls and on the inlet centerbody at the same axial station. Each of the boundary-layer rakes was 1-1/4 inches high and contained five total and one static pressure tube. Special tests were made to measure duct external drag. For these tests, external boundary-layer rakes were mounted at eight azimuth positions 1/4-inch upstream of the duct trailing edge.

TESTING AND PROCEDURE

Three-component force and moment data were obtained through a duct angle range of -4° to +80° and at forward speeds from 0 to about 180 knots. Higher forward speed conditions were simulated by reducing fan speed and operating at the same ratio of fan-tip speed to free-stream velocity as would be obtained at forward speeds greater than 180 knots and at maximum fan speed. Fan speed was varied from about 1200 to about 2400 rpm and was used for thrust control. The method of testing was to vary fan speed independently by varying gas generator (engine) speed and forward speed while maintaining a fixed duct angle. The procedure to define duct inlet stall was to operate at low tip speed ratio (high fan speed) and successively increase tip speed ratio (decrease fan speed) while maintaining a fixed duct angle and forward speed until the inlet stalled. With the duct inlet stalled, tip speed ratio was then decreased by increasing fan speed at the same duct angle and forward speed until the inlet flow reattached. For those tests where external boundary-layer rakes were installed to measure duct external drag, no force or moment data were recorded.

CORRECTIONS

No corrections were applied to the force data to compensate for wind-tunnel wall interference effects with the fan operating as the magnitude of such corrections was not known. Contributions to lift, drag, and pitching moment due to air flowing through the gas generator are included in the data. It should be noted that all gas generator inputs to the data are inherent to the particular system and that placing the gas generator in a remote location would change the lift and moment. The data contain all fan forces as well as aerodynamic forces and include strut interference effects which will be discussed later. All model supports were completely faired and the fairings

were independent of the model and the wind-tunnel force measuring system; hence, no tares for these were applied to the data.

RESULTS

Static Thrust

Static thrust as a function of fan speed is shown in figure 3 for a duct exit area ratio of 1.0.

Aerodynamic Characteristics

Longitudinal aerodynamic characteristics for the configurations tested are presented in figures 4 through 14. The results of figures 4 through 11 are shown in coefficient form and, with the exception of figures 9 and 11, are presented as functions of tip speed ratio and show the effects of forward speed on the model characteristics. Figure 10 shows the effect of duct inlet stall on the model characteristics at duct angles of 50°, 60°, and 70° for a duct exit area ratio of 0.93. Lift-drag characteristics of the model are summarized in figure 12 for ranges of duct angles and fan speeds at several forward speeds. Pitching-moment characteristics as a function of duct angle are summarized in figures 13 and 14 for several fan and forward speeds.

Duct Inlet Pressure Distributions

Representative duct inlet pressures are presented in figures 15 through 17. Figure 15 shows the total pressure loss in the inlet at 0° duct angle both statically and at forward speed. Figures 16 and 17 present inlet radial total pressure distributions at several forward speeds for conditions shortly before and after duct inlet stall.

Performance

The effects of duct exit area and duct external drag on the variation of net thrust with forward speed are presented in figures 18 and 19 (the net thrust includes the external drag of the duct). Figure 20 presents performance estimates in descending flight for a hypothetical airplane (assumed to have two ducted lift-cruise fans as propulsive devices) and shows how the maximum descent rates as a function of forward speed are limited by duct inlet stall for three wing loadings.

DISCUSSION

Static Thrust

The results of the static thrust measurements shown in figure 3 indicate that by extrapolation of the data to 100-percent fan speed with the maximum duct exit area, a value of 7500 pounds of static thrust should be obtained. With a duct exit area ratio of 80 percent of the maximum, the static thrust was reduced by about 18 percent. Further reductions in duct exit area caused engine turbine exhaust temperatures to be higher than permissible for operation at the static conditions; hence, no further static data could be obtained at lower duct exit areas. The inlet total pressure loss measurements shown in figure 15 indicate that a loss greater than 7 percent occurred at static conditions probably as a result of the cambered inlet shape. With very small increases in forward speed, the total pressure loss was reduced to less than 5 percent, and at free-stream dynamic pressures greater than 0.7 of the inlet dynamic pressure, the total pressure loss in the inlet was constant, about 3.5 percent. The measurements of inlet pressure distribution showed that the stagnation pressure on the cambered inlet leading edge moved with forward speed in a manner consistent with the variation of inlet total pressure loss shown in figure 15.

Aerodynamic Characteristics

Lift.- The variation of lift coefficient with forward speed at 0° duct angle was generally small (figs. 4 through 8). Lift developed with increasing duct angle. Figure 11 shows that lift was due both to the free-stream flow over the duct and to loads induced by fan speed. Lift contributions at duct angles greater than 0° were also due to the component of thrust in the lift direction which increased with increasing duct angle.

Pitching moment.- Increases in positive pitching moment accompanied increases in duct angle. The results of figure 11 show that an unstable pitching-moment slope was characteristic of the duct itself in the absence of engine power effects. The pitching moment maintains an unstable slope to high lift coefficients and becomes large with increasing fan speed at high duct angles. It should be noted, however, that the large positive pitching moments are partially the result of the choice of moment center at the duct pivot on the fan axis at 45.8 percent of the duct chord. Placing the moment center at 25-percent duct chord would reduce the moment arm and cause lower positive pitching moments. This is illustrated in figure 14 for the pitching-moment variations shown in figure 13 at 80 and 121 knots forward speed and at 2200 rpm fan speed.

Duct inlet stall.- The duct inlet did not stall at duct angles of 40° and less. The results in figure 10 show losses in lift and thrust and reductions of positive pitching moments with duct inlet stall. A hysteresis-stall loop resulted when fan speed was decreased until the inlet stalled and then

increased until the inlet flow reattached (fig. 10). A small increase in fan speed at constant throttle setting accompanied inlet stall.

Radial total-pressure distributions upstream of the fan showed that at all of the duct angles at which the inlet stalled, flow separation was restricted to the lower portion of the inlet and was evident across the entire inlet radius (figs. 16 and 17).

Performance

The data of figures 4 through 8 indicated that tip speed ratio appeared to be a good correlating independent parameter that would allow extrapolation of test data to higher fan and forward speeds. The curves presented in figures 18 and 19 scale test data obtained at lower fan and forward speeds to higher forward speeds on the basis of tip speed ratio for 100-percent fan speed (2640 rpm). Such scaling of test data should be effective until independent Mach number effects are encountered.

Duct exit area variation.- The highest thrust was obtained with a duct exit area ratio of 1.0 up to forward speeds of about 190 knots (fig. 18). The highest thrust at forward speeds greater than about 230 knots was obtained with a duct exit area ratio of 0.74. At forward speeds greater than about 290 knots there was little difference in net thrust for exit area ratios of 0.62 and 0.74. A duct exit area ratio of 0.80 showed a slight thrust superiority over the small forward speed range between about 190 knots and 230 knots. Increases in duct exit area greater than an exit area ratio of 0.74 caused progressively lower thrust values at higher forward speeds. A lower limit of duct exit area seemed to have been exceeded with an exit area ratio of 0.56 which generally produced a low level of net thrust over most of the speed range.

Duct external drag.- Integration of boundary-layer total pressures at the duct trailing edge, measured with the power on, showed a high over-all duct external drag coefficient of 0.11. Those rakes mounted on the relatively clean bottom of the duct indicated much lower local values of duct external drag coefficient, approximately 0.04. The results of figure 18 are for a duct external drag coefficient of about 0.11. If the external drag could be reduced to about 0.04, gains in net thrust could be achieved over the entire range of forward speeds. This is illustrated in figure 19 for two exit area ratios. This figure shows that for an exit area ratio of 0.62, reducing the external drag coefficient from 0.11 to 0.04 would allow the maximum forward speed for zero net thrust to be increased from about 362 knots to about 430 knots. The gains in performance obtainable by reducing the external duct drag are greater for the smaller duct exit area required at cruise speeds than for the larger duct exit area required for zero and low forward speeds. The limit of such performance improvements is demonstrated by the case of zero external drag.

Tuft observations and boundary-layer measurements indicated that the high external duct drag was attributable in part to large areas of rough and separated flow over the duct surface downstream of the strut mounts. This external flow interference was due to the presence of the horizontal fairings and to the proximity to the duct wall of the vertical strut fairings. Another factor thought to adversely affect the duct external flow was the severe duct surface contour changes downstream of the fan on the upper half of the duct. Increased thickness on this portion of the duct was necessary to enclose the ducting system that delivered the jet exhaust to the tip turbine. This increased duct thickness resulted in larger trailing-edge closure angles (angle between inner and outer duct surfaces) on the upper half of the duct.

Inlet stall boundaries.- The performance estimates presented in figure 20 are for a hypothetical airplane assumed to have a wing aspect ratio of 4.0, a wing area of 300 square feet, and two tilting ducted lift-cruise fans as propulsive devices. Wing loadings of 40, 50, and 60 lb/sq ft used for these computations correspond to thrust-to-weight ratios of 1.25, 1.00, and 0.83, respectively, (based on 15,000 pounds of net static thrust available from the two ducted lift-cruise fans at 100-percent fan speed). Constant values of wing C_L and C_D of 1.20 and 0.20, respectively, were assumed for the airplane at all forward speeds exclusive of any duct contributions. The maximum descent rates possible for the airplane as limited by duct inlet stall varied from approximately 1160 ft/min at 80° duct angle and 40 lb/sq ft wing loading to about 2150 ft/min at 50° duct angle and 60 lb/sq ft wing loading (fig. 20).

Duct inlet stall depends upon the duct angle and fan speed or power required at any forward speed; however, the airplane maximum descent performance also depends upon the portion of the load carried by the wing. A reduction of the wing lift coefficient from the values of 1.20 assumed for the descent calculations has the immediate effect of increased fan speed or power required to carry the additional load and results in increased descent capability.

Ames Research Center
National Aeronautics and Space Administration
Moffett Field, Calif., Aug. 17, 1964

REFERENCES

1. Anon. Results of Static Tests of a Full Scale, Wing Mounted, Tip Turbine Driven Lift Fan. The General Electric Co., Flight Propulsion Lab. Dept., TCREC-TR-62-21, March 1962.

2. Aoyagi, Kiyoshi, Hickey, David H., and deSavigny, Richard A.: Aerodynamic Characteristics of a Large-Scale Model With a High Disk-Loading Lifting Fan Mounted in the Fuselage. NASA TN D-775, 1961.

3. deSavigny, Richard A., and Hickey, David H.: Aerodynamic Characteristics in Ground Effect of a Large-Scale Model With a High Disk-Loading Lifting Fan Mounted in the Fuselage. NASA TN D-1557, 1963.

4. Goldsmith, Robert H., and Hickey, David H.: Characteristics of Lifting-Fan V/STOL Aircraft. Astronautics and Aerospace Engineering, vol. 1, no. 9, Oct. 1963, pp. 70-77.

5. Hickey, David H., and Hall, Leo P.: Aerodynamic Characteristics of a Large-Scale Model With Two High Disk-Loading Fans Mounted in the Wing. NASA TN D-1650, 1963.

TABLE I.- DUCT COORDINATES

(a) Internal and external contours

Internal contour, leading edge through station 68.00					
X, inches	Y, inches	X, inches	Y, inches	X, inches	Y, inches
0.70	28.30	21.07	25.08	47.16	29.16
.90	27.21	23.07	25.36	48.16	29.31
1.16	26.72	25.07	25.63	49.16	29.45
1.40	26.46	27.07	25.91	50.16	29.60
2.08	25.86	29.07	26.21	51.16	29.73
3.00	25.38	31.07	26.52	52.16	29.87
4.00	25.04	32.16	26.69	53.16	29.99
5.00	24.78	33.16	26.85	54.16	30.12
6.00	24.56	34.16	27.01	55.16	30.24
7.00	24.41	35.16	27.17	56.16	30.36
8.00	24.30	36.16	27.33	57.16	30.47
9.00	24.23	37.16	27.49	58.16	30.58
10.25	24.20	38.16	27.66	59.16	30.68
11.07	24.21	39.16	27.83	60.16	30.78
12.07	24.22	40.16	28.00	61.16	30.87
13.07	24.26	41.16	28.17	62.16	30.96
14.07	24.32	42.16	28.33	63.16	31.03
15.07	24.41	43.16	28.50	64.16	31.10
16.07	24.50	44.16	28.67	65.16	31.17
17.07	24.61	45.16	28.83	66.16	31.21
19.07	24.84	46.16	28.99	68.00	31.25

External contour	
Station 68.00 to 152.47	
β, deg	radius, R, in.
16	219.50
20	226.46
30	240.82
40	257.71
50	280.90
60	317.41
68	384.22
90 to 180	486.43

TABLE I.- DUCT COORDINATES - Concluded

(b) External contours

External contour, leading edge through station 68.00, Y, in.								
X, inches	Circumferential position from top of duct, deg							
	16	20	30	40	50	60	68	90 to 180
0.70	28.30	28.30	28.30	28.30	28.30	28.30	28.30	28.30
.90	29.57	29.54	29.47	29.41	29.34	29.24	29.12	29.00
1.24	30.53	30.47	30.36	30.25	30.12	29.95	29.74	29.53
1.40	30.95	30.88	30.75	30.62	30.46	30.27	30.01	29.76
1.78	31.67	31.58	31.42	31.25	31.05	30.80	30.48	30.16
2.32	32.33	32.23	32.03	30.82	31.59	31.29	30.90	30.52
2.86	32.90	32.78	32.55	32.31	32.05	31.71	31.27	30.84
3.40	33.41	33.28	33.02	32.76	32.47	32.29	31.60	31.12
4.08	34.02	33.88	33.59	33.30	32.97	32.55	32.00	31.46
5.44	35.05	34.87	34.53	34.19	33.80	33.30	32.66	32.02
6.80	35.96	35.76	35.38	34.99	34.55	33.99	33.25	32.53
8.16	36.80	36.58	36.16	35.73	35.24	34.61	33.79	32.99
10.20	37.90	37.65	37.18	36.69	36.13	35.42	34.50	33.60
13.60	39.48	39.19	38.64	38.07	37.42	36.60	35.52	34.47
17.00	40.85	40.53	39.90	39.26	38.54	37.62	36.41	35.22
20.40	42.06	41.70	41.02	40.33	39.53	38.52	37.20	35.89
23.80	43.16	42.78	42.04	41.29	40.42	39.33	37.90	36.50
27.20	44.15	43.74	42.95	42.15	41.23	40.06	38.54	37.05
34.00	45.84	45.38	44.51	43.63	42.60	41.31	39.63	37.97
40.80	47.20	46.70	45.76	44.71	43.71	42.32	40.51	38.73
47.60	48.23	47.70	46.71	45.71	44.55	43.09	41.17	39.29
54.40	48.95	48.40	47.38	46.34	45.15	43.62	41.64	39.69
61.20	49.38	48.83	47.78	46.72	45.50	43.95	41.92	39.93
68.00	49.51	48.95	47.90	46.83	45.60	44.04	42.00	40.00

TABLE II.- CENTERBODY GEOMETRY

Inlet centerbody	
X, inches	Y, inches
31.07	0
31.33	1.17
31.55	1.60
31.88	2.09
32.52	2.89
33.67	4.01
36.23	5.90
39.13	7.45
43.32	9.19
49.12	10.92
55.57	12.16
60.73	12.67
62.02	12.72
63.31	12.75
64.37	12.75
68.00	12.75
Leading-edge radius = 2.80	

Exit centerbody			
X, inches	Y, inches		
	$\frac{A_e}{A_{e,s}} = 0.6$	$\frac{A_e}{A_{e,s}} = 0.8$	$\frac{A_e}{A_{e,s}} = 1.0$
73.75	12.50	12.50	12.50
108.92	12.50	12.50	12.50
109.97	12.60	12.51	12.50
111.22	12.70	12.60	12.50
112.47	12.80	12.65	12.50
114.97	13.30	12.85	12.51
117.47	14.05	13.25	12.55
119.97	15.05	13.75	12.55
124.97	17.50	15.30	12.55
129.97	19.80	16.65	12.55
134.97	21.40	17.75	12.60
137.97	21.90	18.05	12.60
139.97	22.25	18.35	12.65
142.47	22.35	18.40	12.65
144.97	22.35	18.40	12.60
147.47	22.30	18.35	12.55
147.97	22.05	18.25	12.40
152.47*	21.65	17.95	12.35
154.97	21.20	17.60	12.29
187.47	12.35	11.80	11.25
189.97	11.70	11.40	11.10
191.22	11.35	11.15	11.00
192.47	11.00	10.90	10.80
193.72	10.70	10.65	10.60
194.97	10.35	10.35	10.35
222.47	2.95	2.95	2.95
225.17	0	0	0

*Duct trailing edge

Note:
1. Frame containing fan from station 68.00 to station 73.75.
2. Increase X dimensions of exit centerbodies by 8 inches for exit area ratios of 0.56, 0.74, and 0.93.

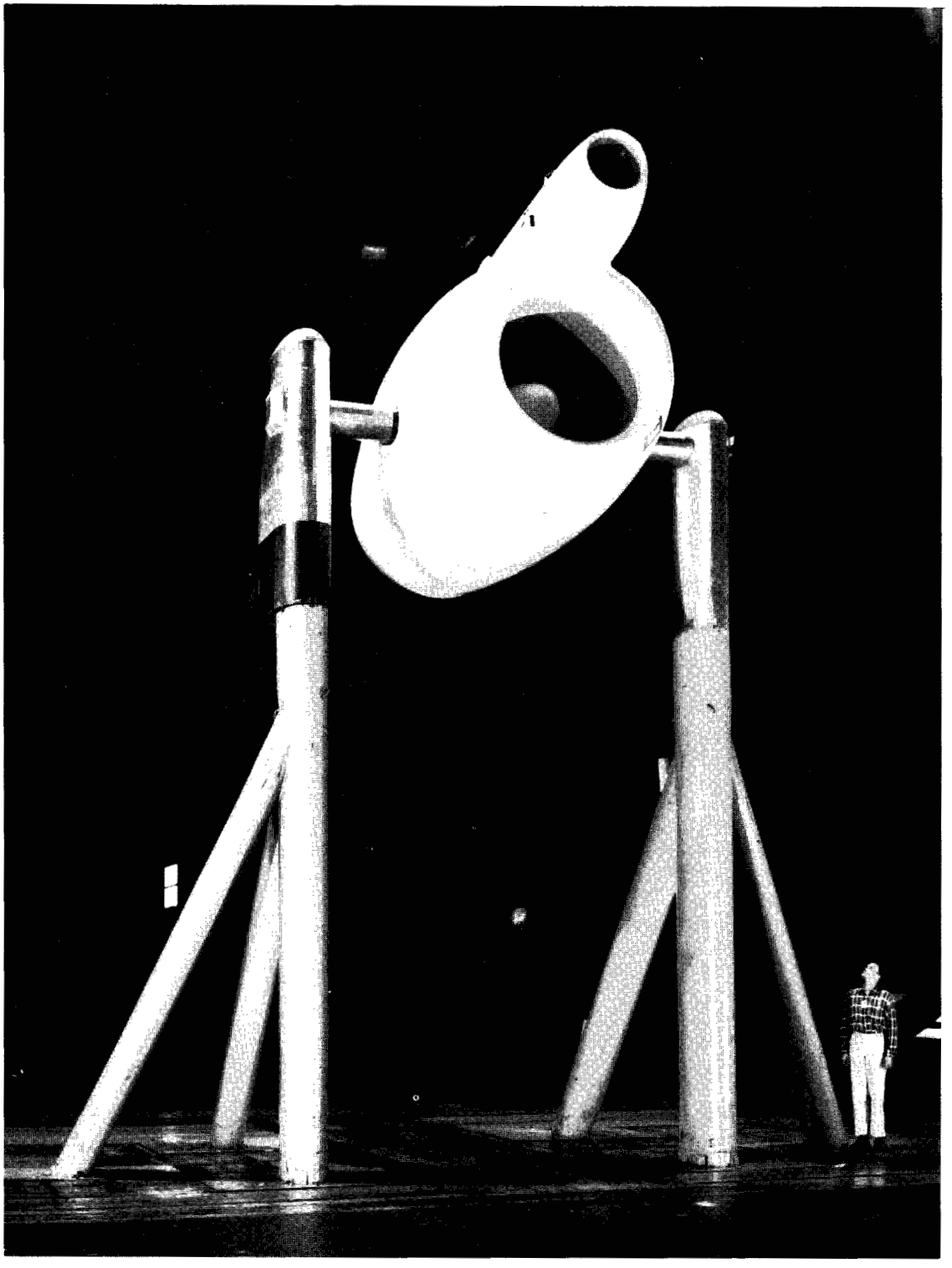

A-31081

(a) Front view of model.

Figure 1.- Model mounted in the test section of the Ames 40- by 80-foot wind tunnel.

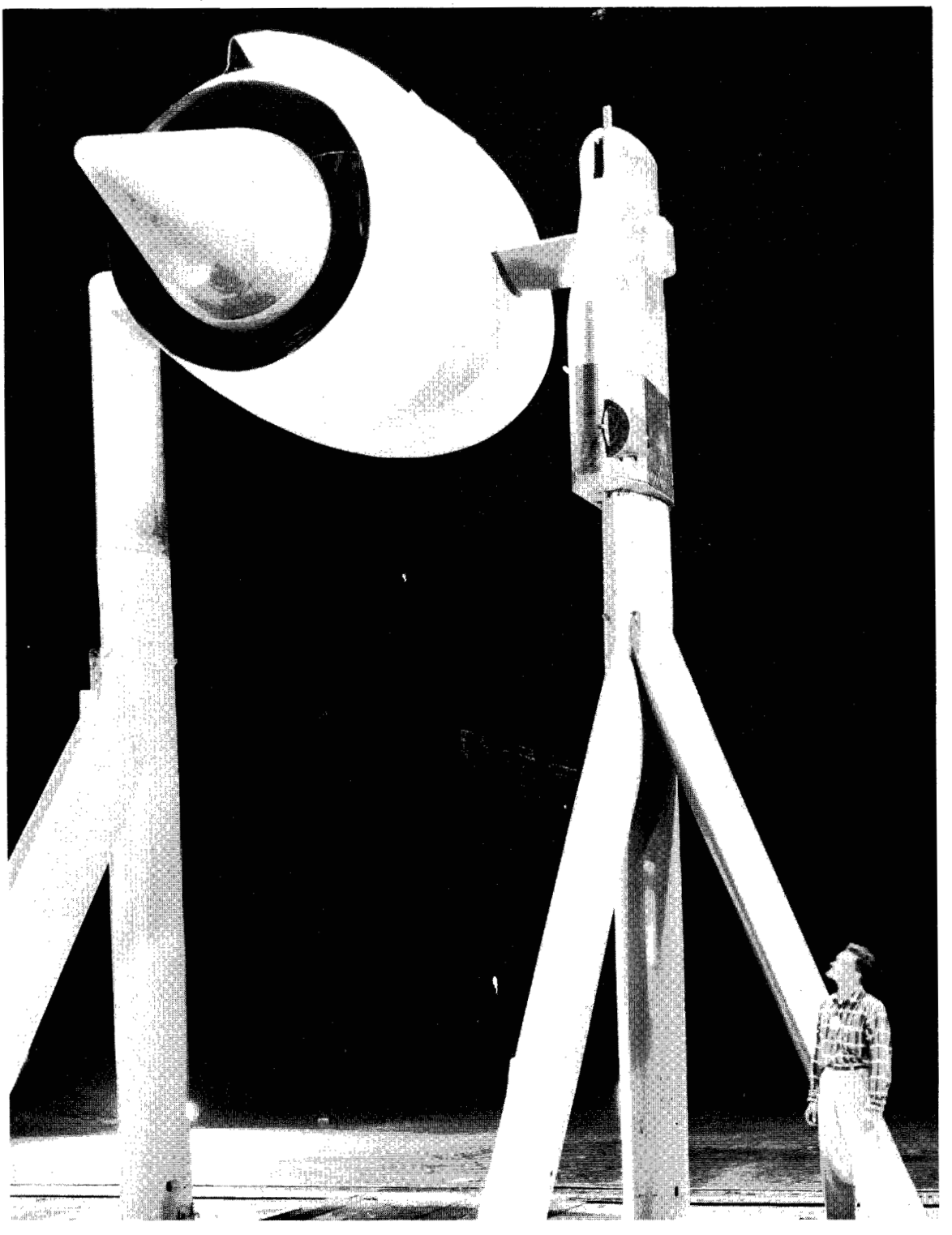

A-31082

(b) Rear view of model showing duct exit with diffuser centerbody installed giving cruise exit area ($A_e/A_{e,s}$ = 0.62).

Figure 1.- Concluded.

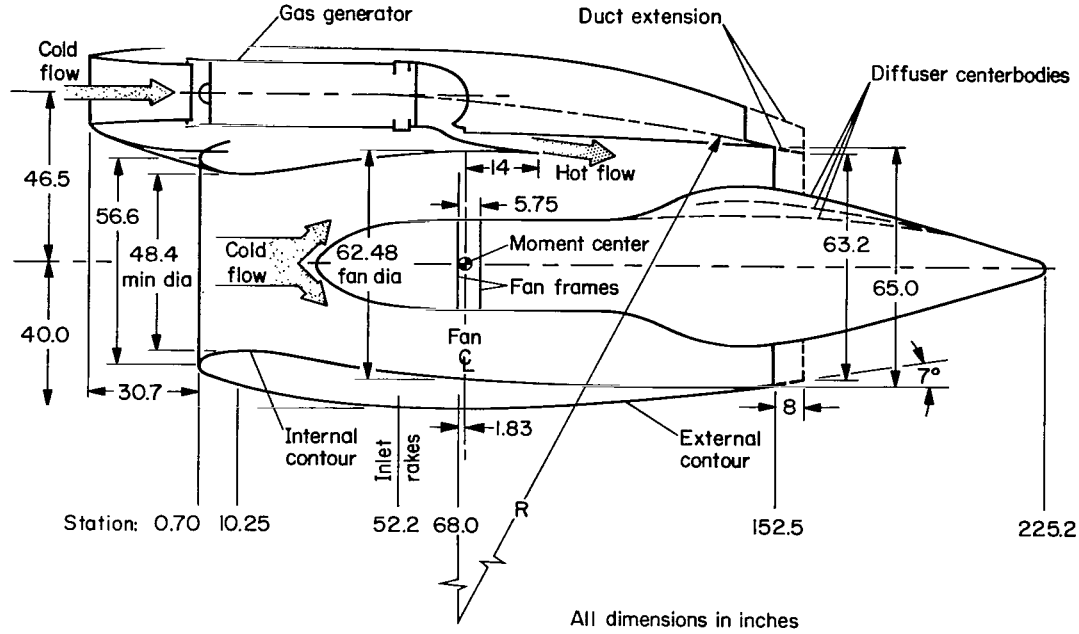

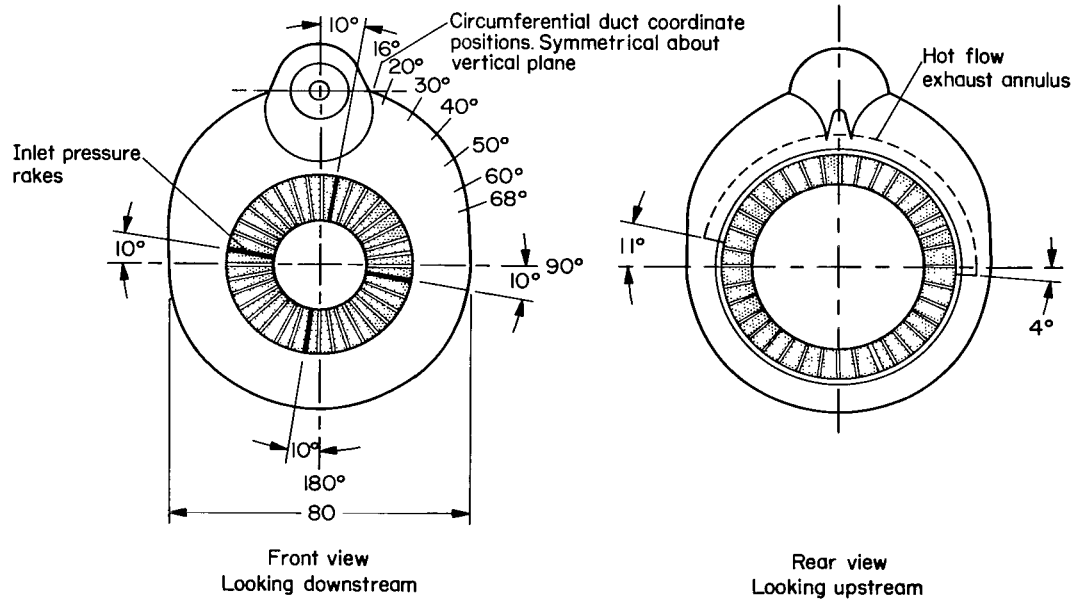

Front view
Looking downstream

Rear view
Looking upstream

Exit area sq ft	Exit area Ratio
19.57	1.00
15.67	.80
12.16	.62
18.28*	.93
14.44*	.74
10.95*	.56
*Lengthened duct	

Figure 2.- Model dimensions and geometry.

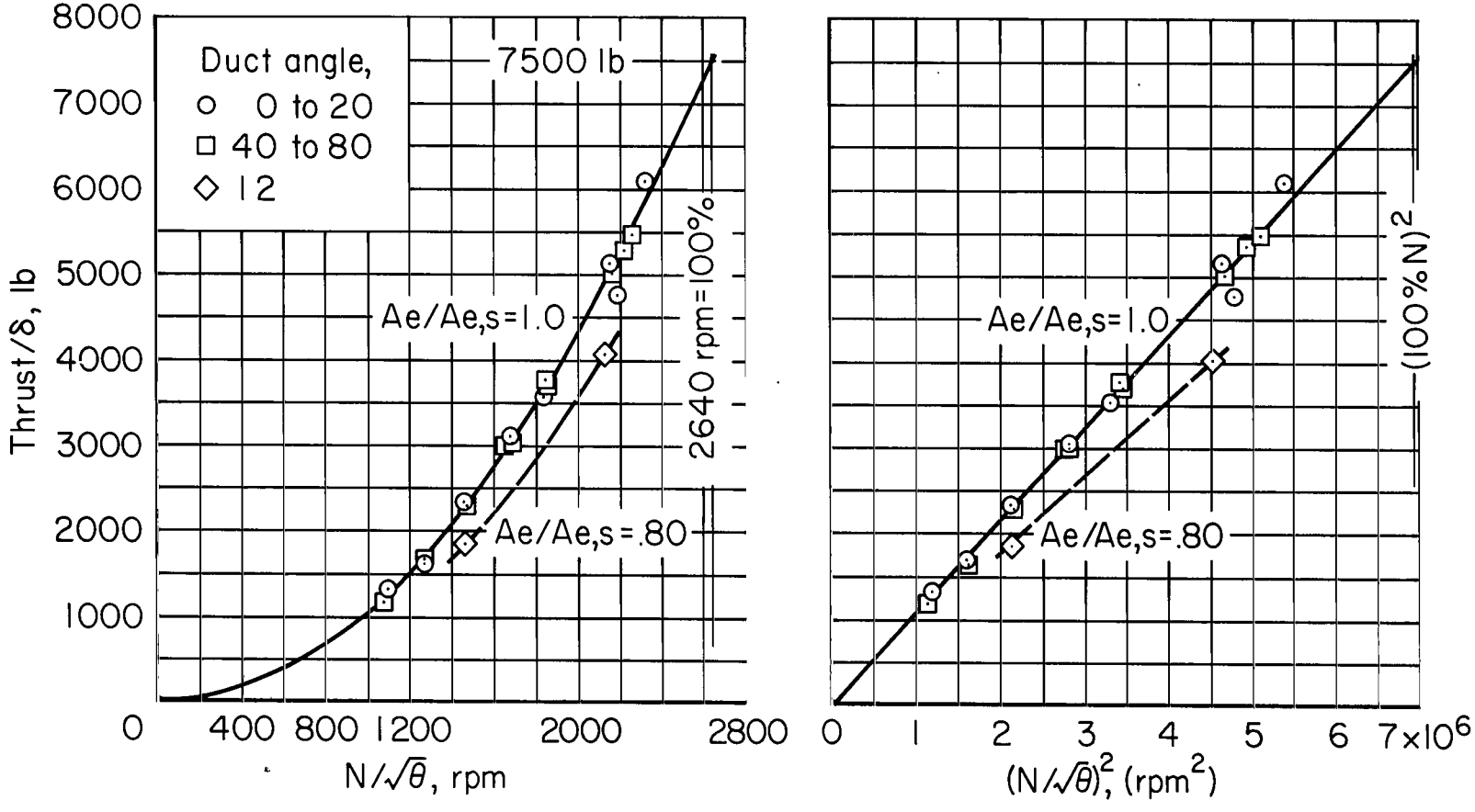

Figure 3.- Fan performance at zero forward speed with the fan installed in the duct.

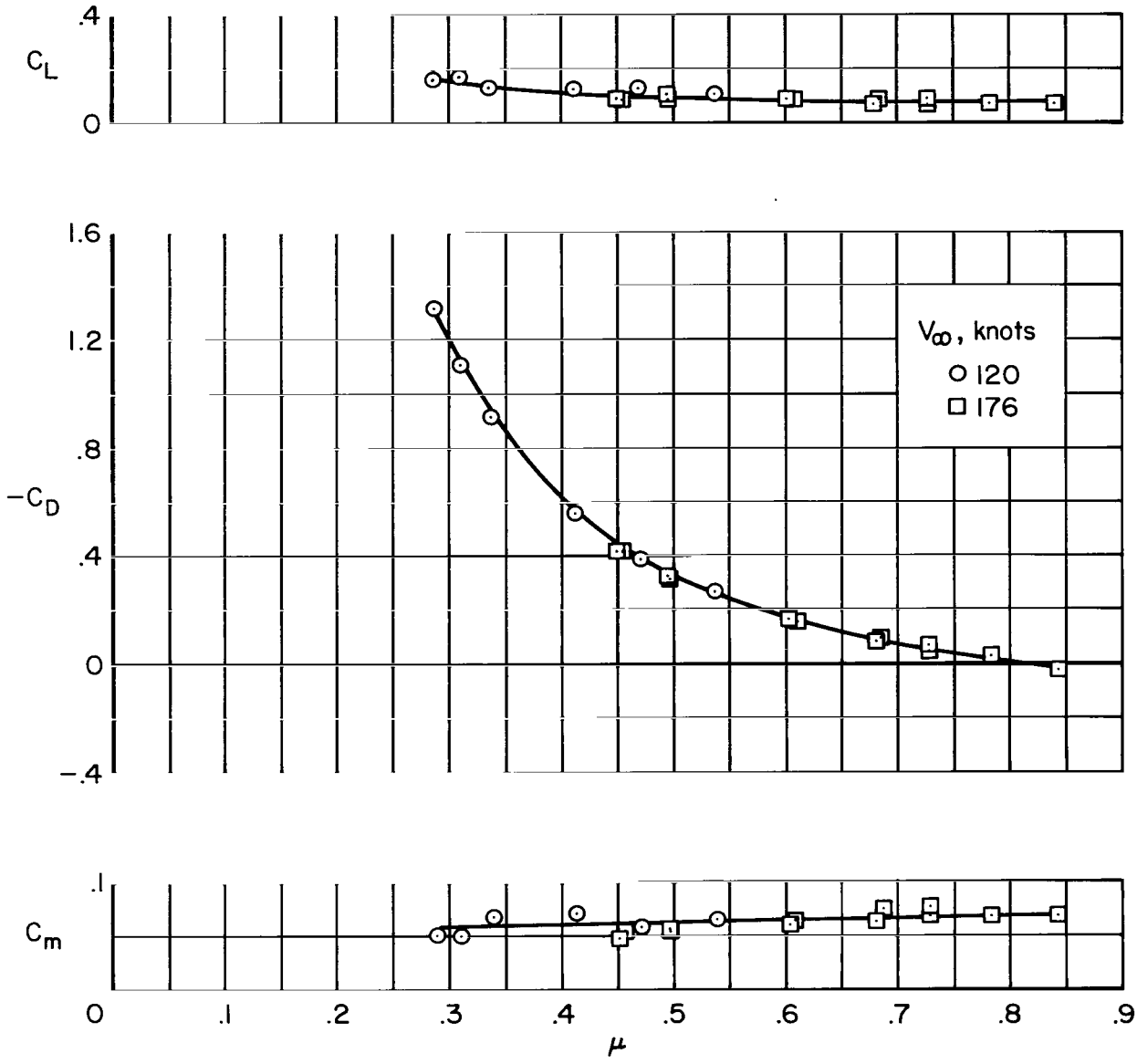

Figure 4.- Variation of model longitudinal aerodynamic characteristics with fan tip speed ratio; $\alpha = 0^\circ$, $A_e/A_{e,s} = 0.56$.

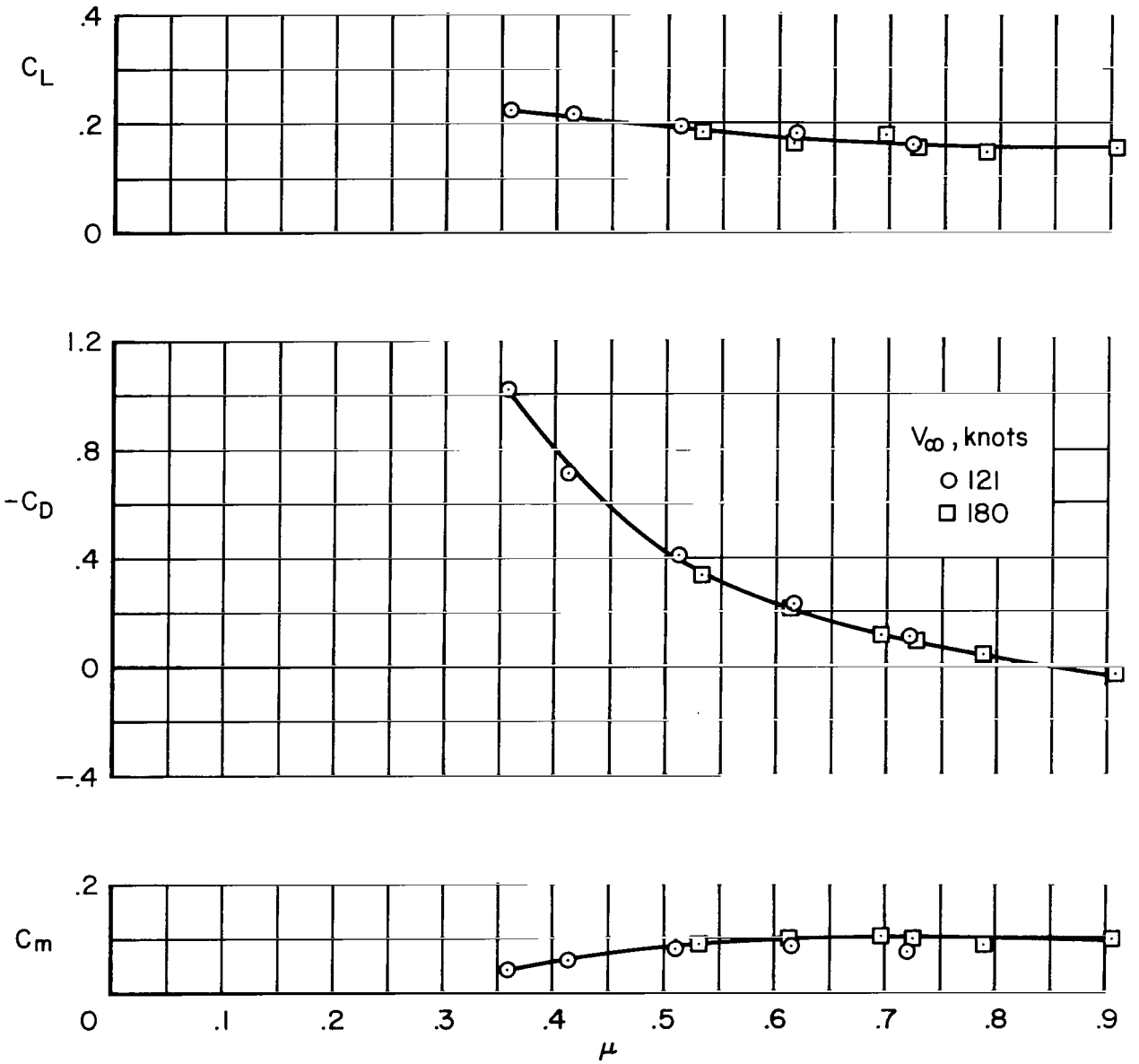

Figure 5.- Variation of model longitudinal aerodynamic characteristics with fan tip speed ratio; $\alpha = 0^\circ$, $A_e/A_{e,s} = 0.62$.

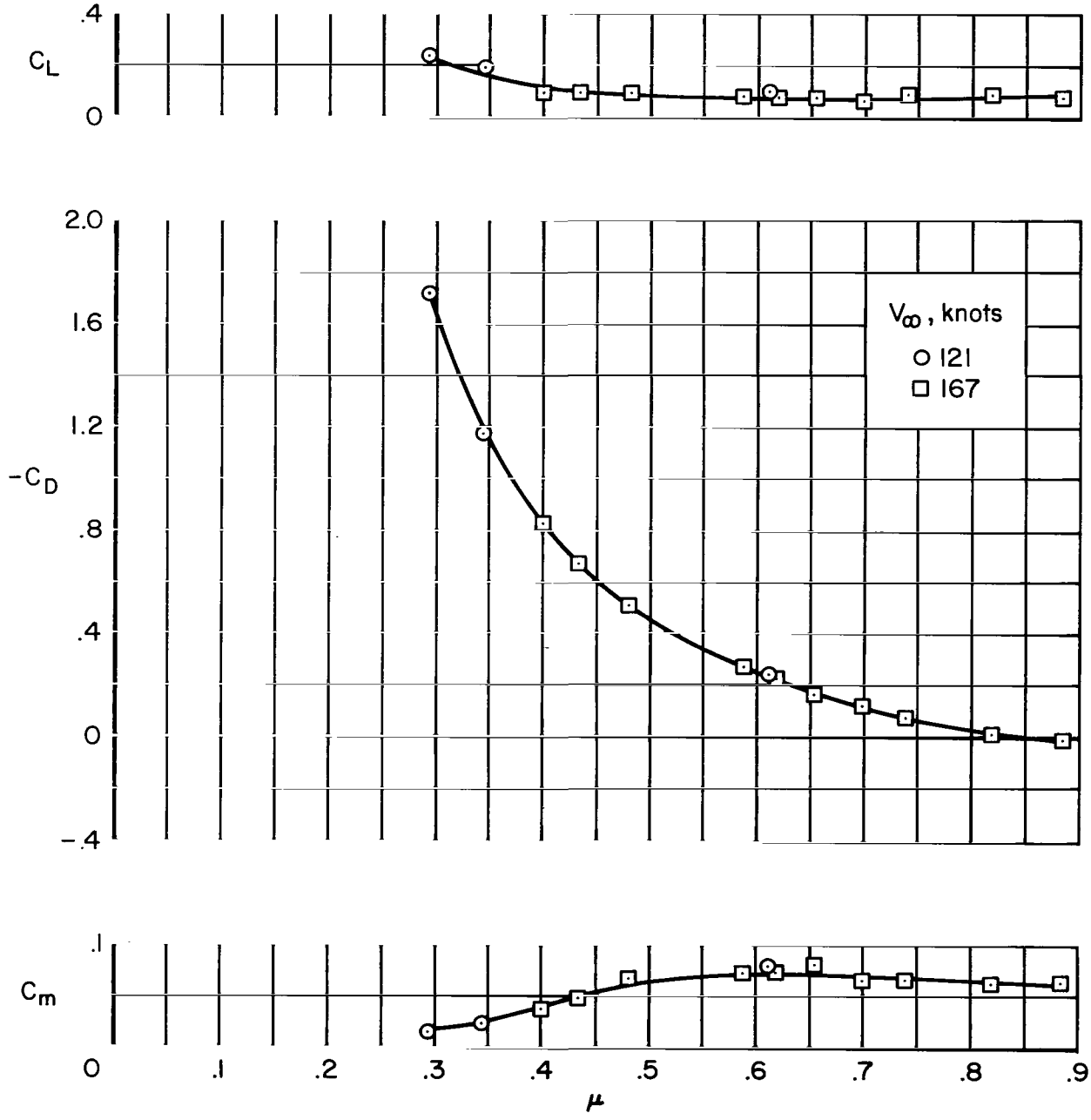

Figure 6.- Variation of model longitudinal aerodynamic characteristics with fan tip speed ratio; $\alpha = 0^\circ$, $A_e/A_{e,s} = 0.74$.

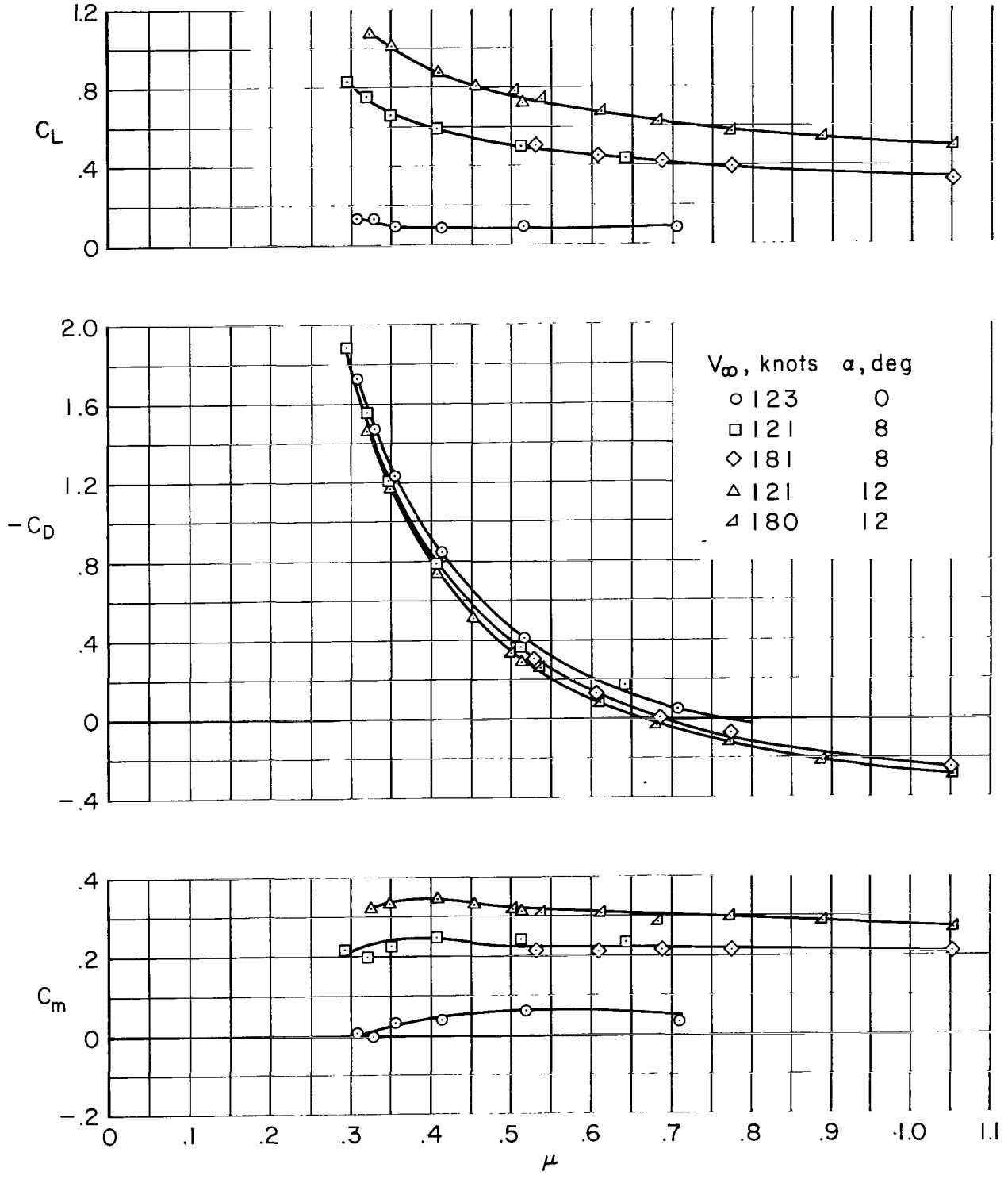

Figure 7.- Variation of model longitudinal aerodynamic characteristics with fan tip speed ratio; $A_e/A_{e,s} = 0.80$.

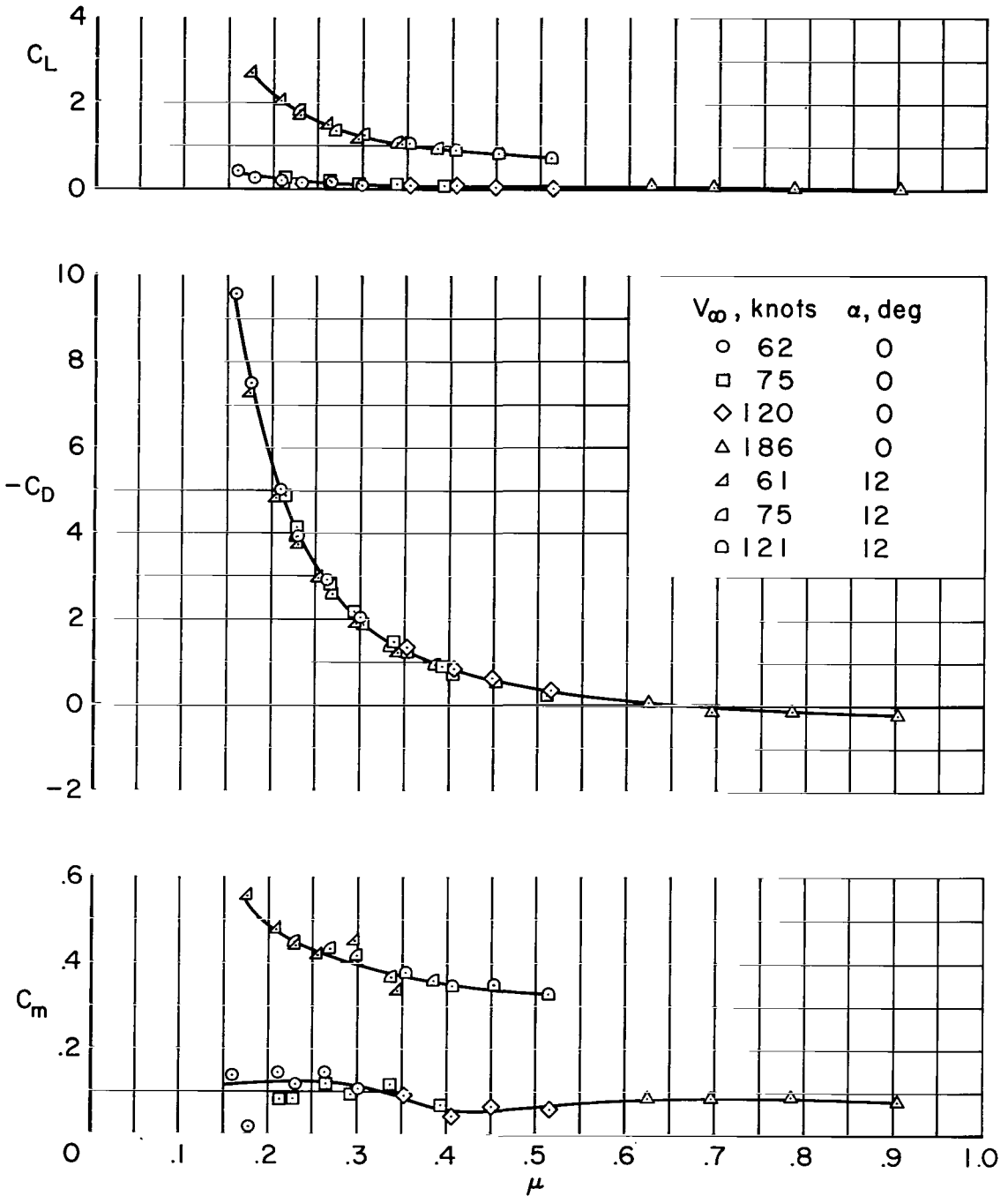

(a) $\alpha = 0^\circ$ and 12°

Figure 8.- Variation of model longitudinal aerodynamic characteristics with fan tip speed ratio; $A_e/A_{e,s} = 1.0$.

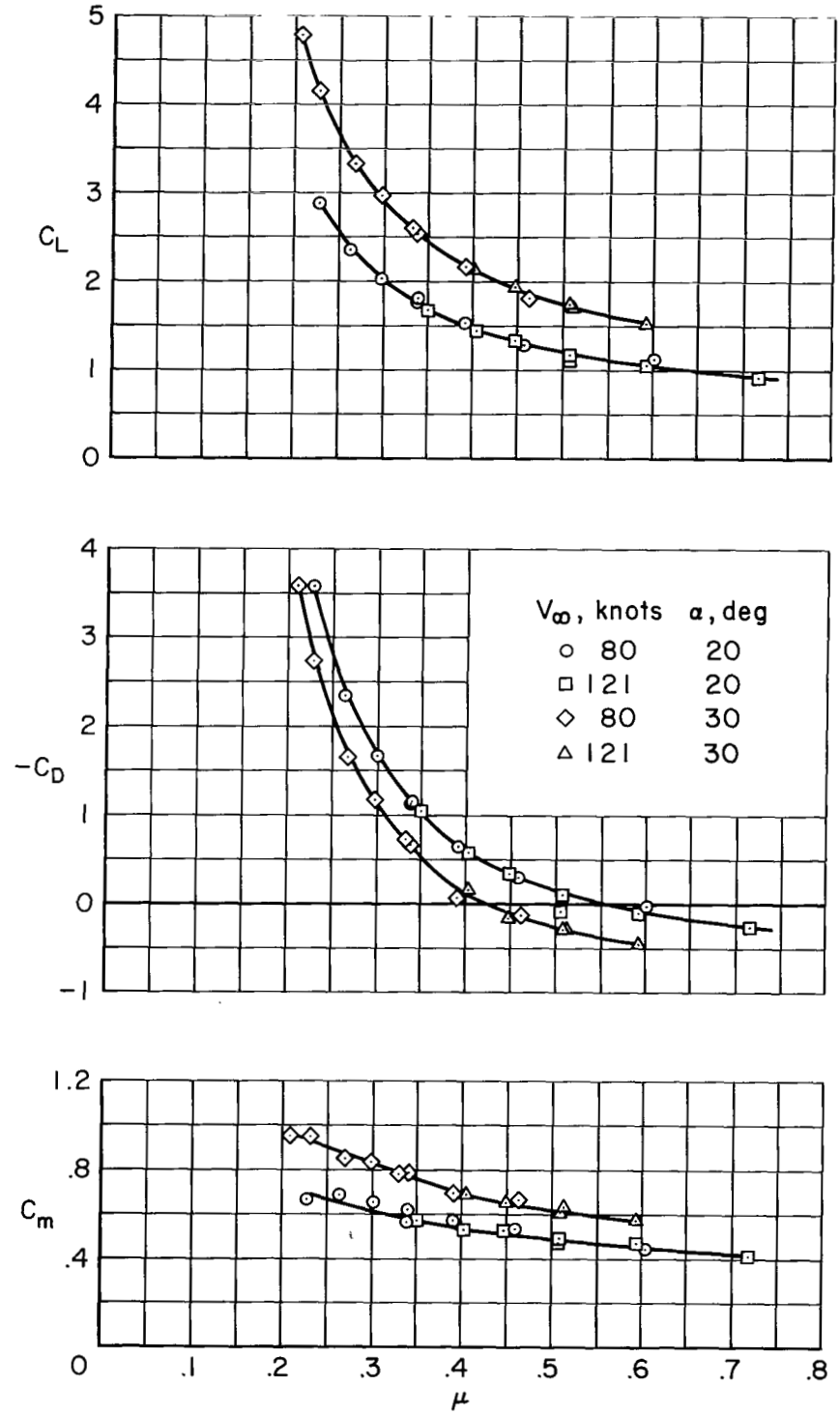

(b) $\alpha = 20^\circ$ and 30°

Figure 8.- Continued.

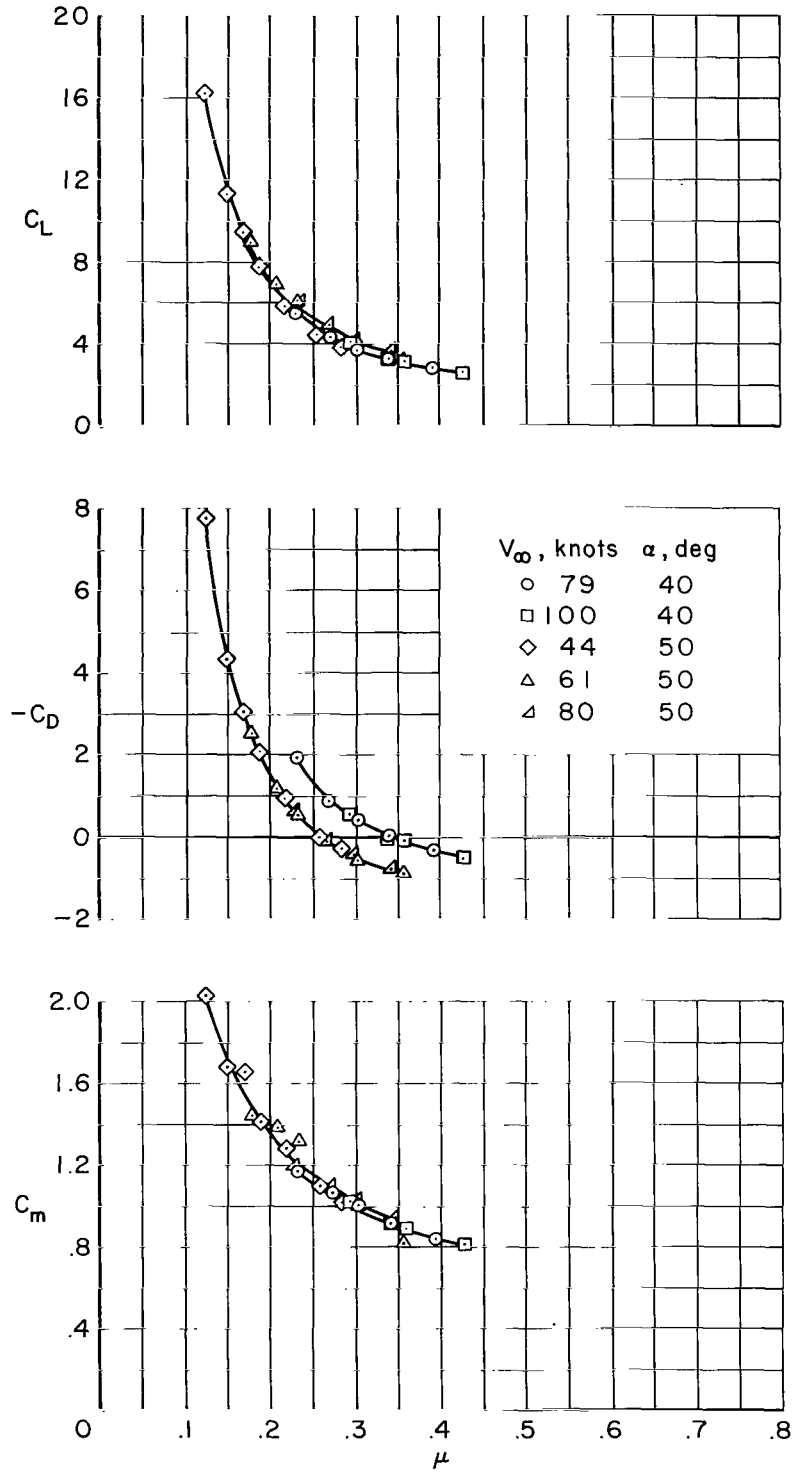

(c) $\alpha = 40^\circ$ and 50°

Figure 8.- Continued.

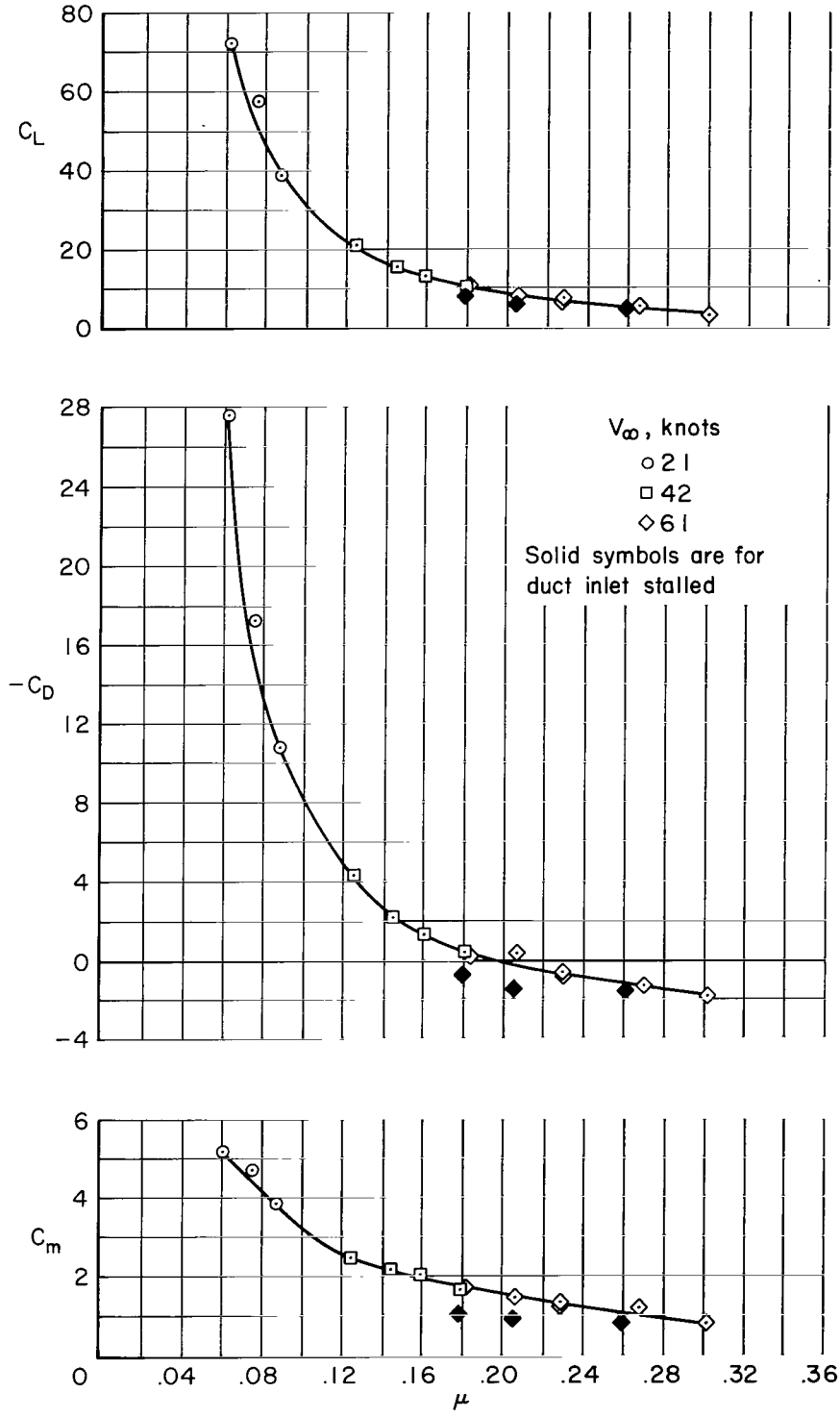

(d) $\alpha = 60^\circ$

Figure 8.- Concluded.

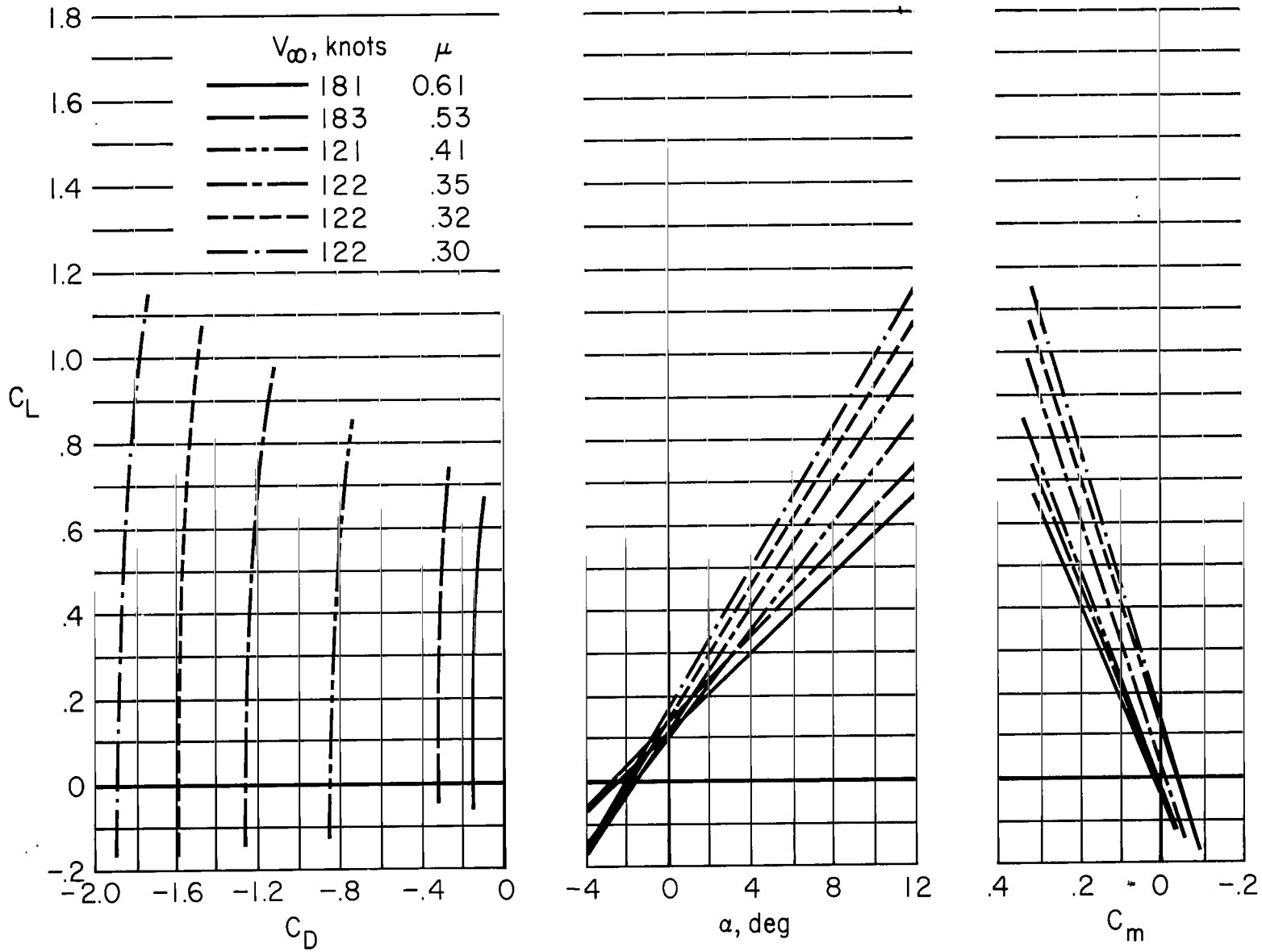

Figure 9.- Model longitudinal aerodynamic characteristics with the fan operating; $A_e/A_{e,s}$ = 0.80.

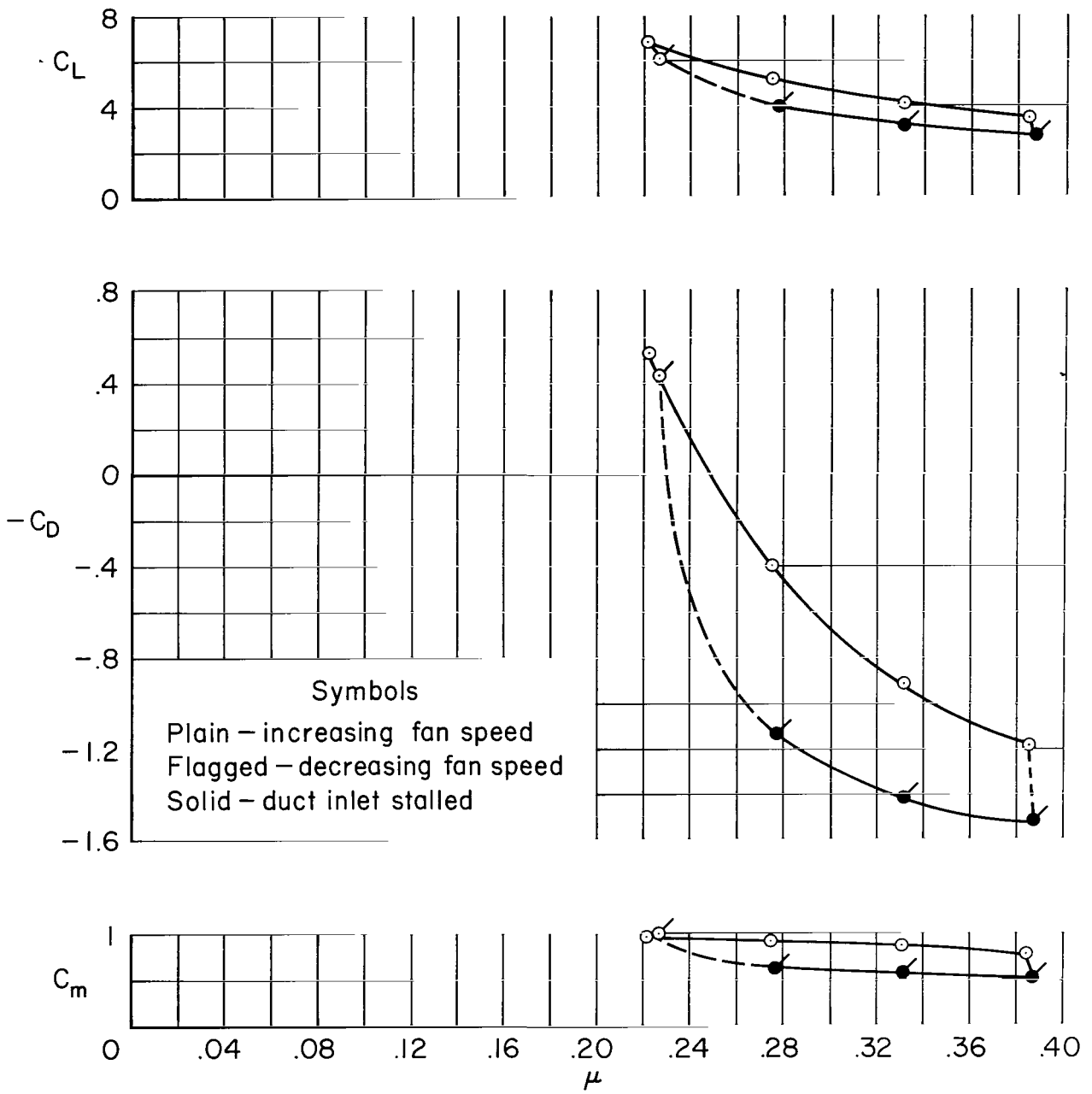

(a) $\alpha = 50^{\circ}$, $V_{\infty} = 79$ knots.

Figure 10.- Effect of duct inlet stall on the variation of model longitudinal aerodynamic characteristics with fan tip speed ratio; $A_e/A_{e,s} = 0.93$.

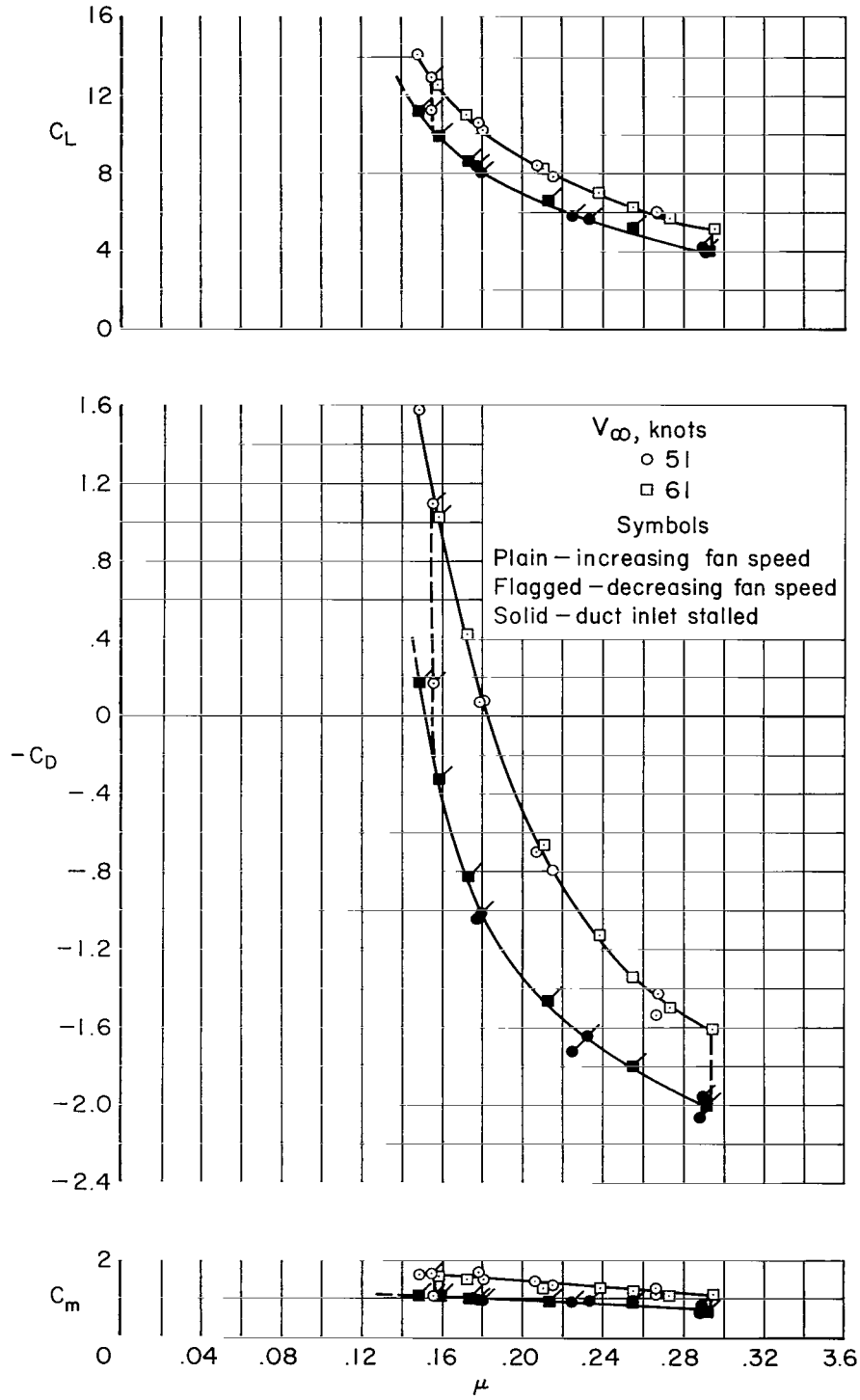

(b) $\alpha = 60^\circ$

Figure 10.- Continued.

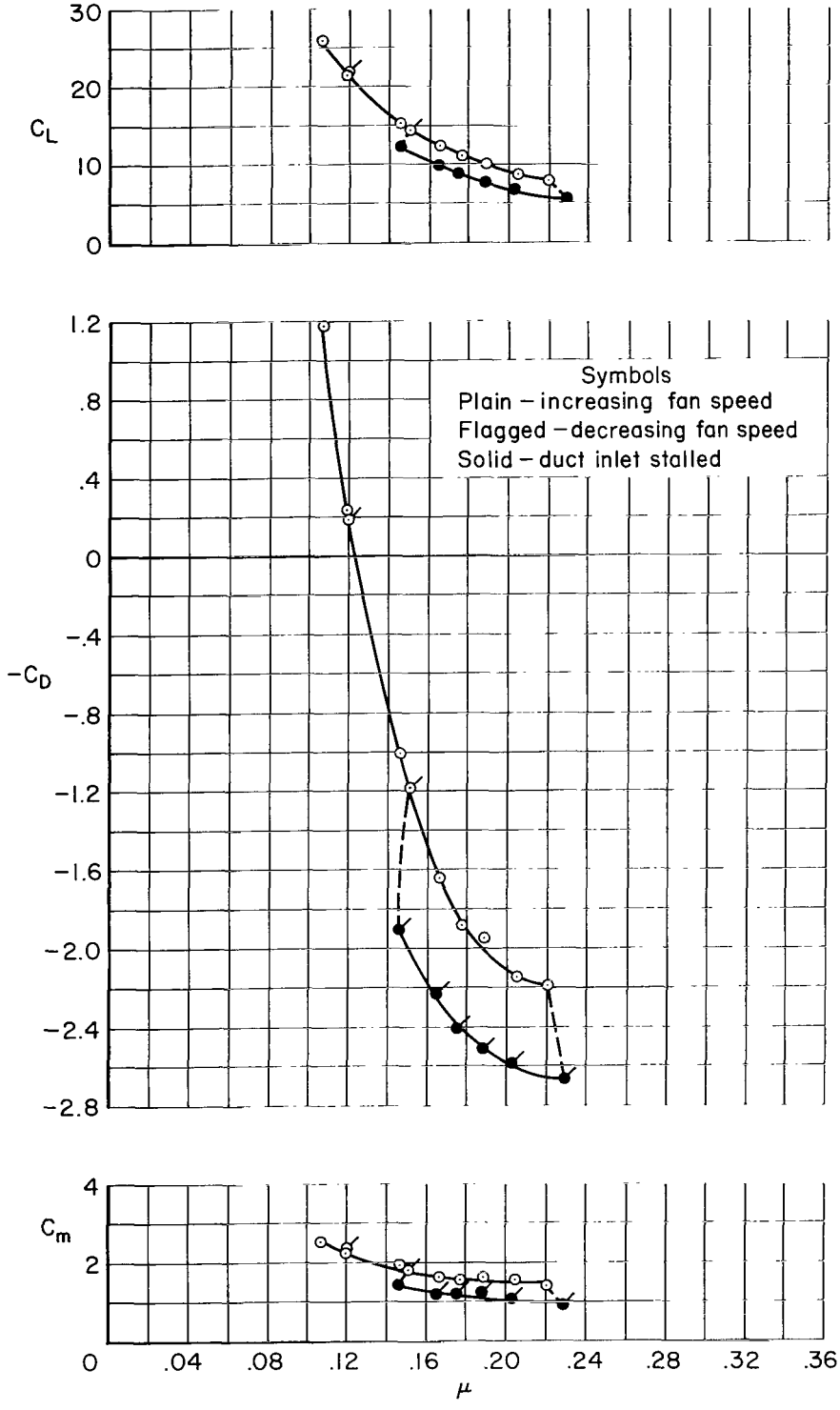

(c) $\alpha = 70^{\circ}$, $V_{\infty} = 42$ knots.

Figure 10.- Concluded.

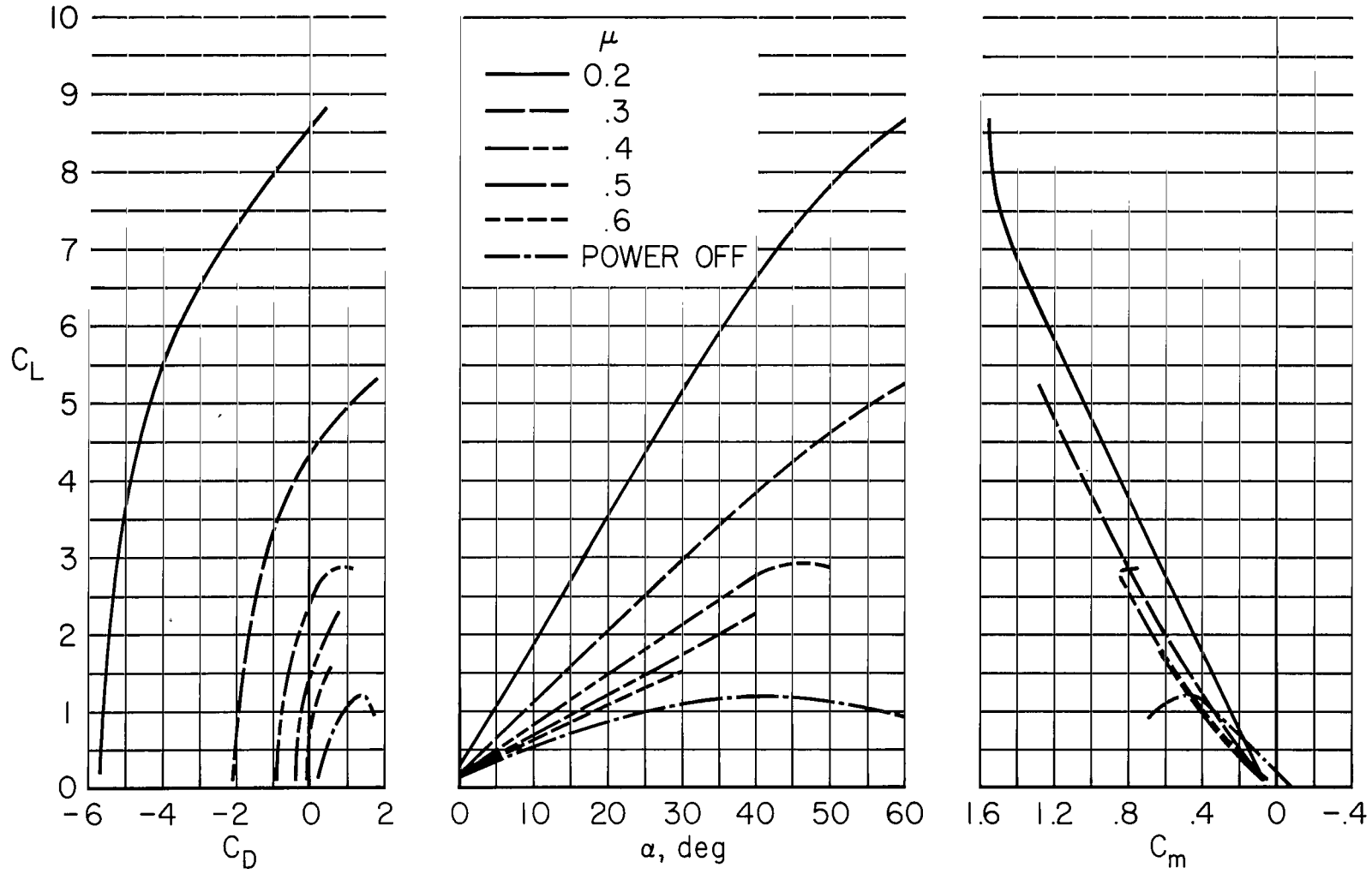

Figure 11.- Model longitudinal aerodynamic characteristics with the fan operating; $A_e/A_{e,s} = 1.0$.

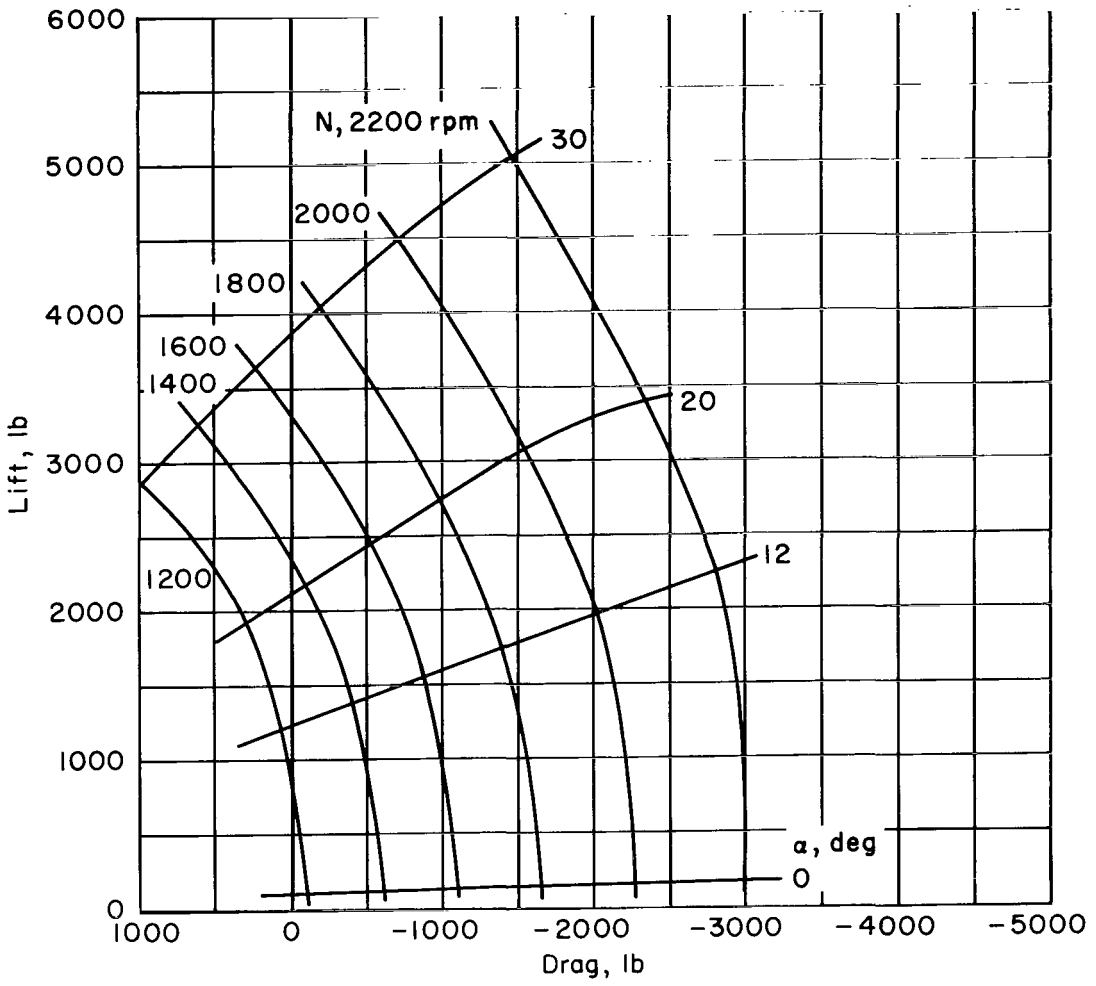

(a) V_∞ = 121 knots.

Figure 12.- Longitudinal force characteristics of the model; $A_e/A_{e,s}$ = 1.0.

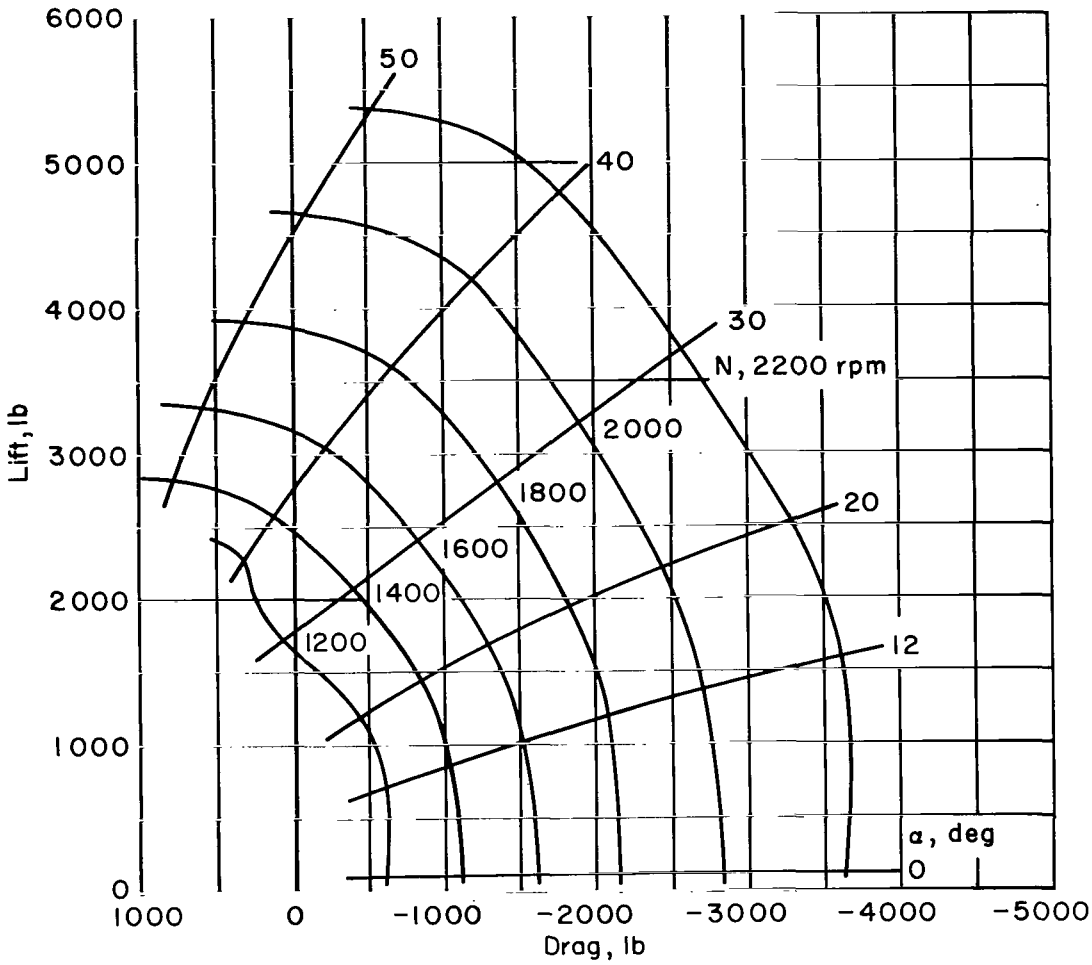

(b) V_∞ = 80 knots.

Figure 12.- Continued.

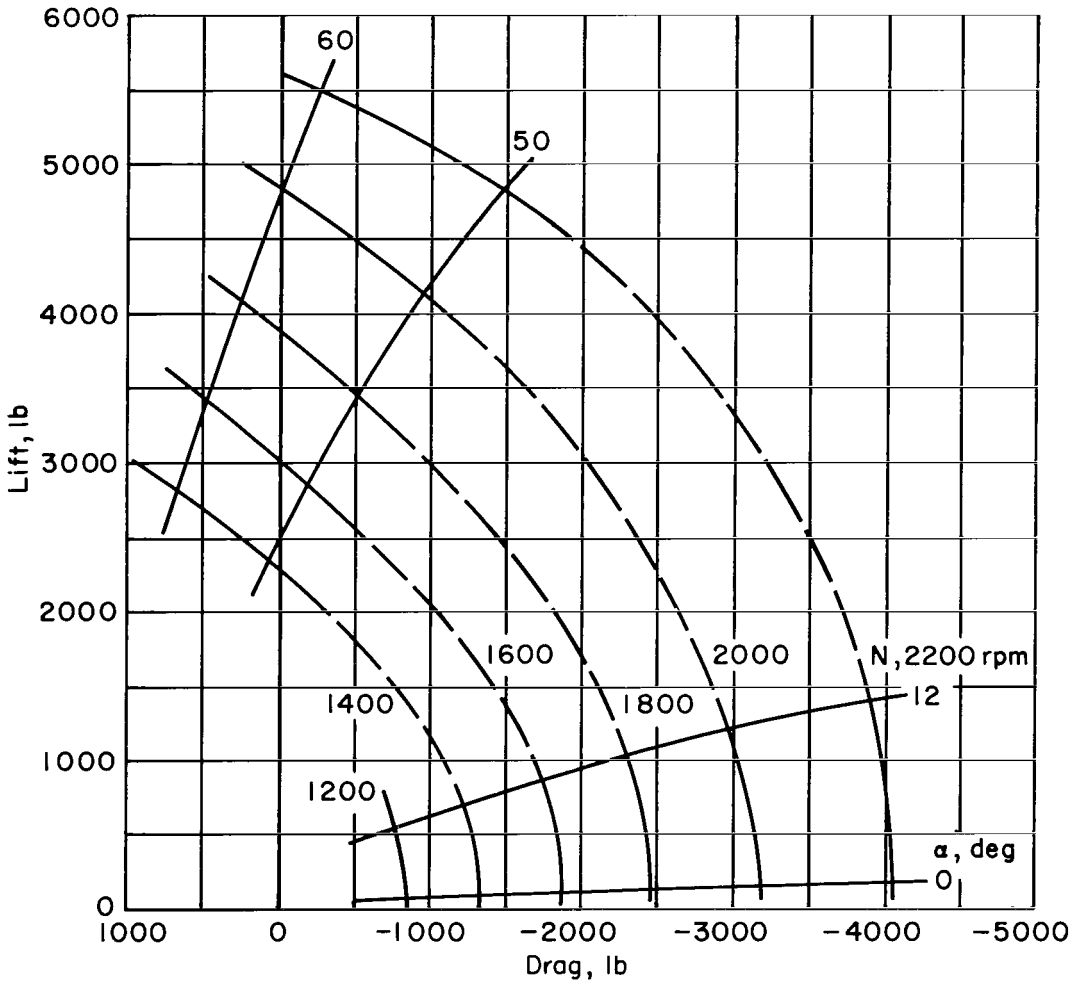

(c) V_∞ = 61 knots.

Figure 12.- Continued.

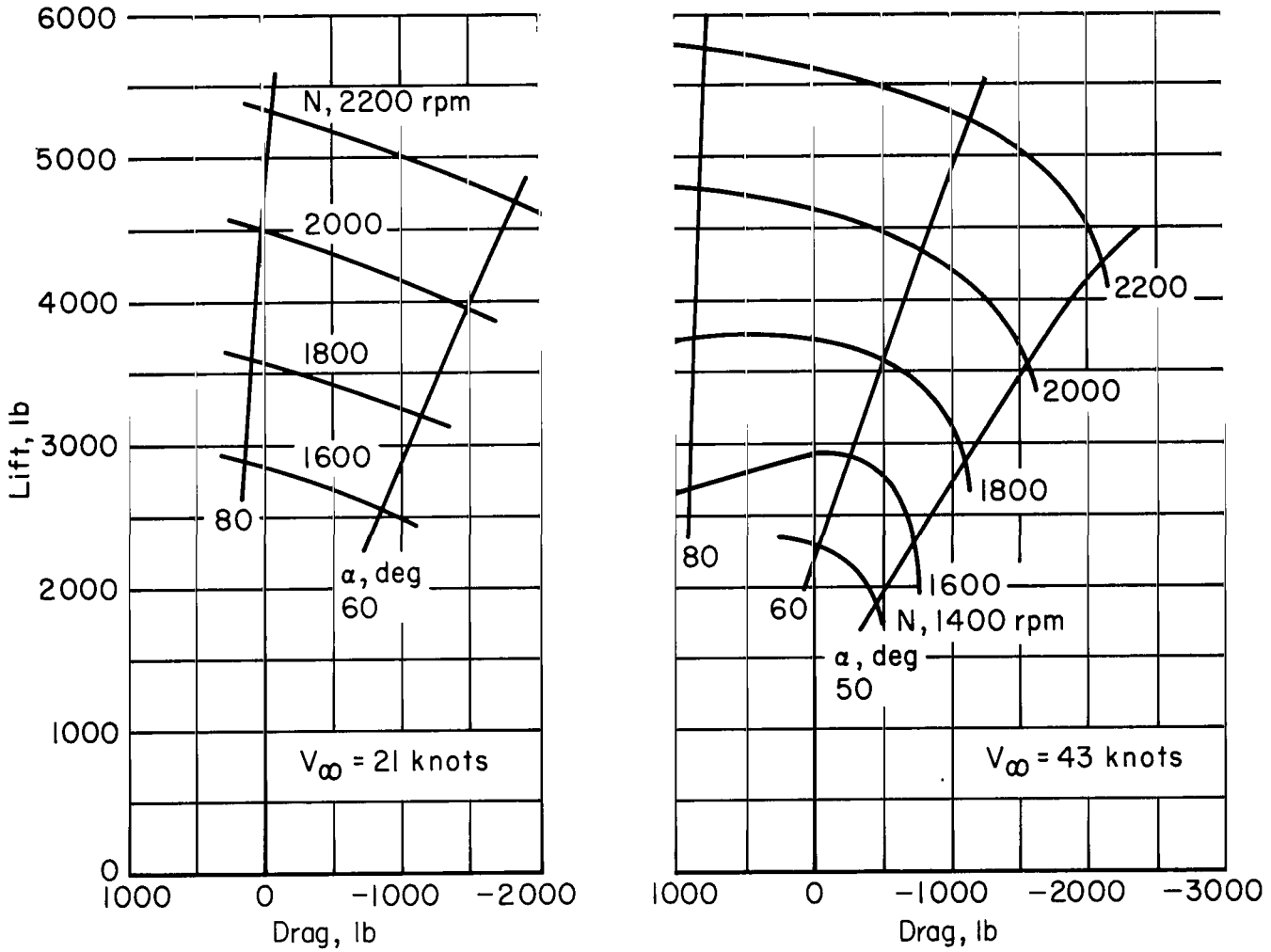

(d) V_∞ = 21 and 43 knots.

Figure 12.- Concluded.

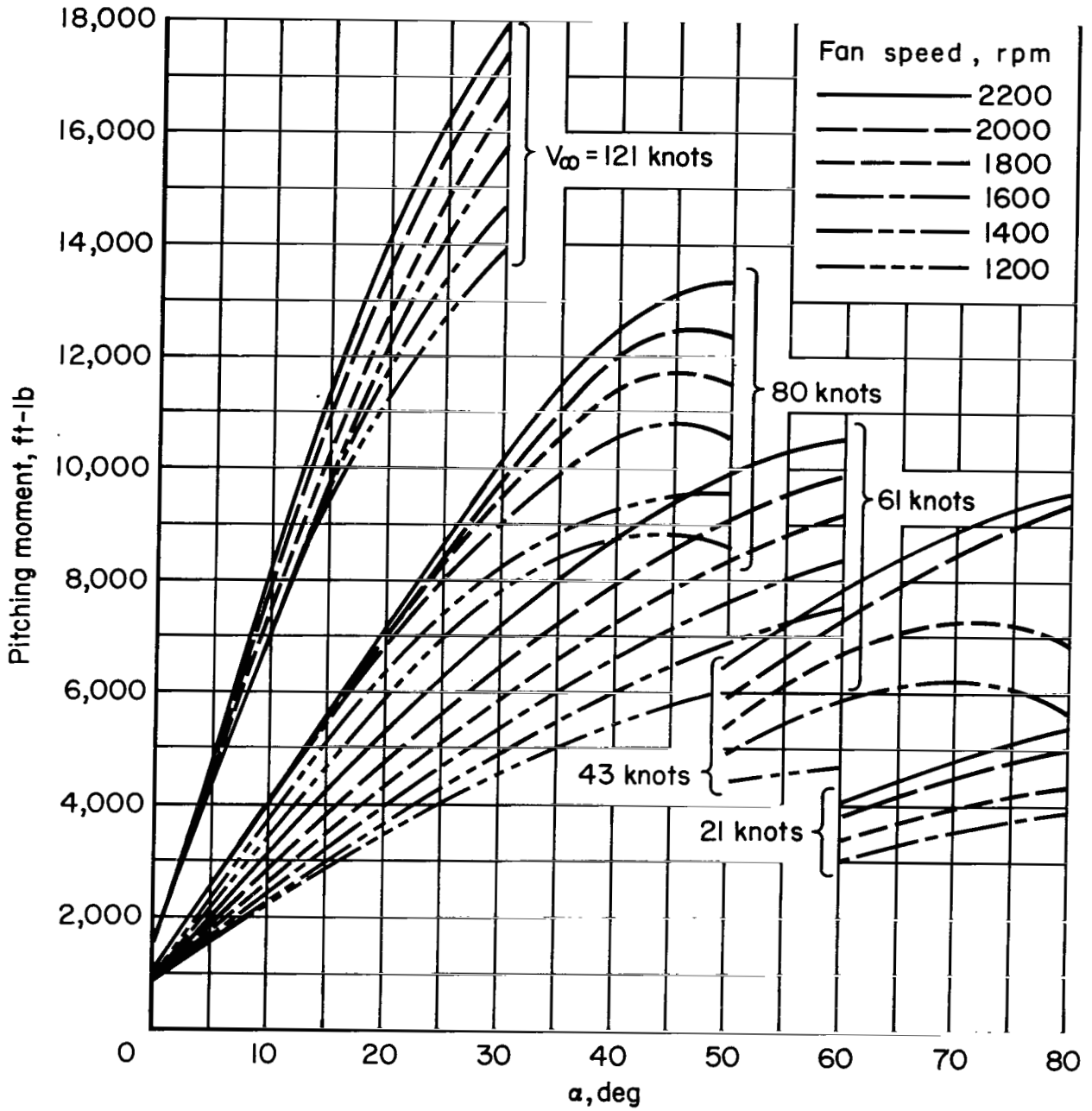

Figure 13.- Variation of pitching moment about model moment center with duct angle and forward speed; $A_e/A_{e,s} = 1.0$.

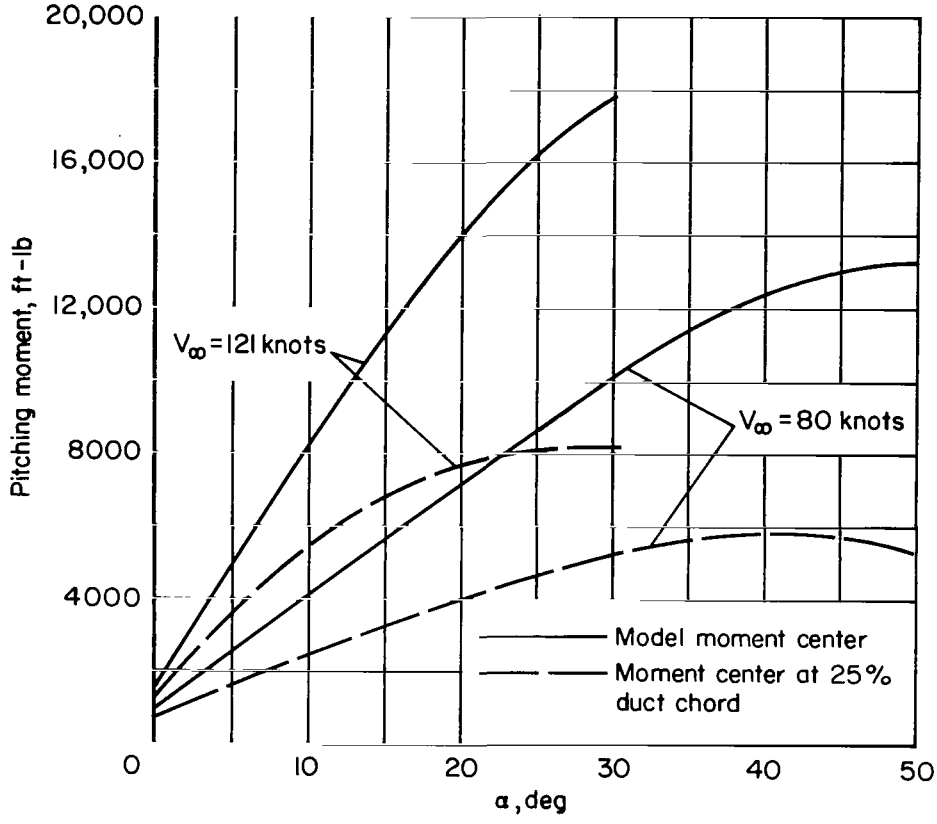

Figure 14.- Variation of pitching moments about model moment center and about a moment center at 25-percent duct chord; $A_e/A_{e,s} = 1.0$, N = 2200 rpm.

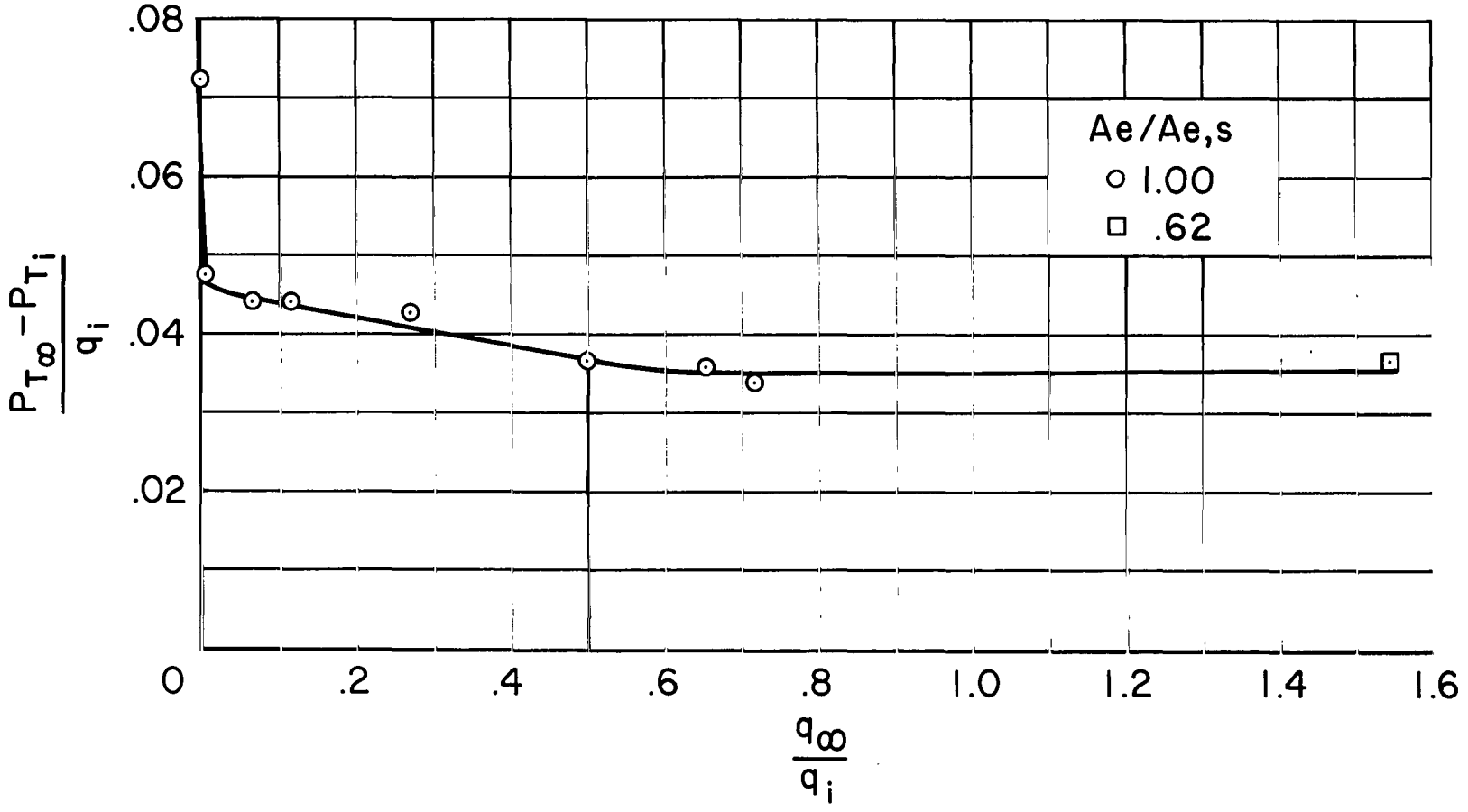

Figure 15.- Variation of duct inlet total pressure loss with forward speed; $\alpha = 0^{o}$.

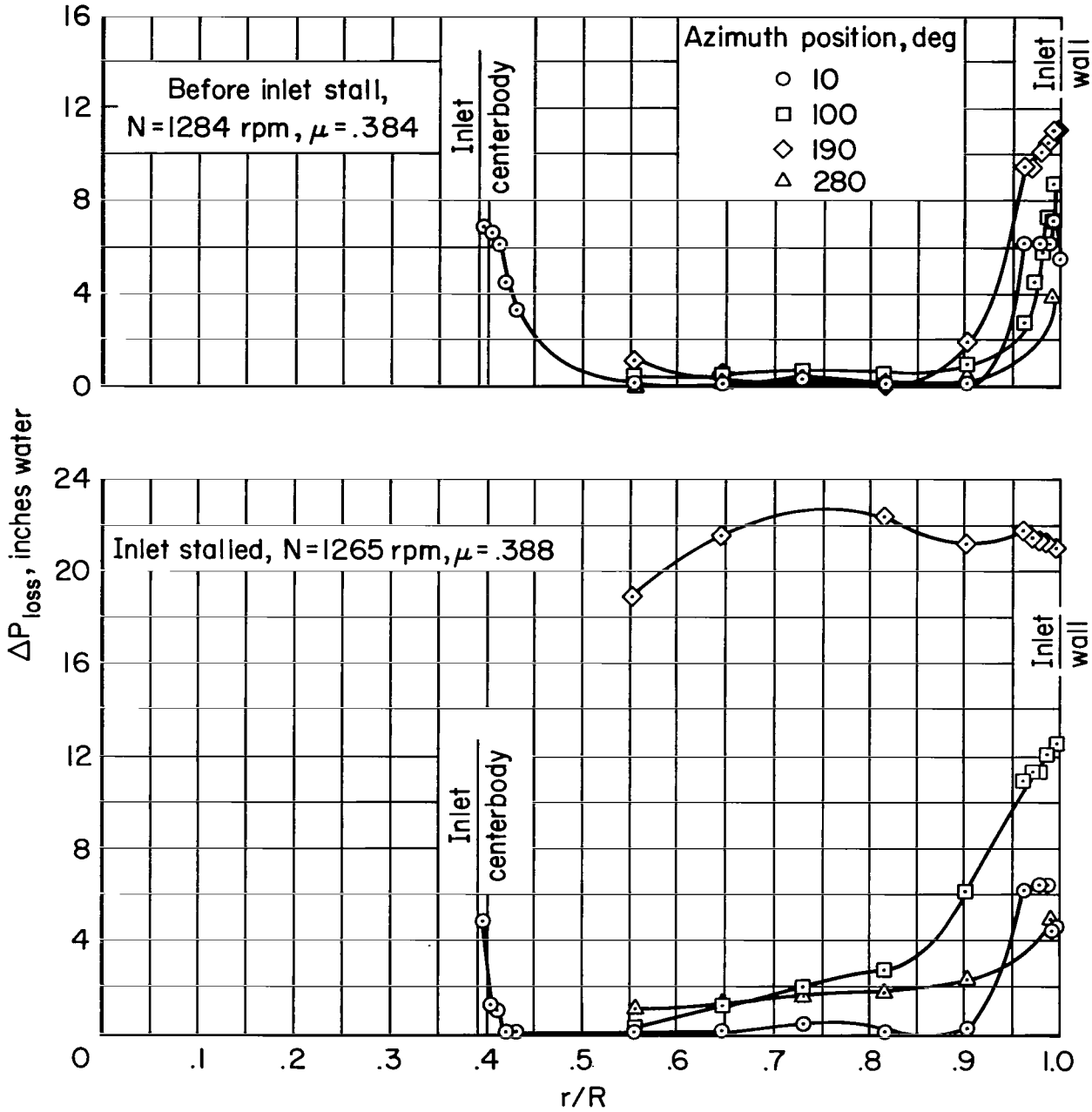

(a) $\alpha = 50^{\circ}$, $V_{\infty} = 79$ knots.

Figure 16.- Effect of duct inlet stall on the radial total pressure distribution in the inlet; $A_e/A_{e,s} = 0.93$.

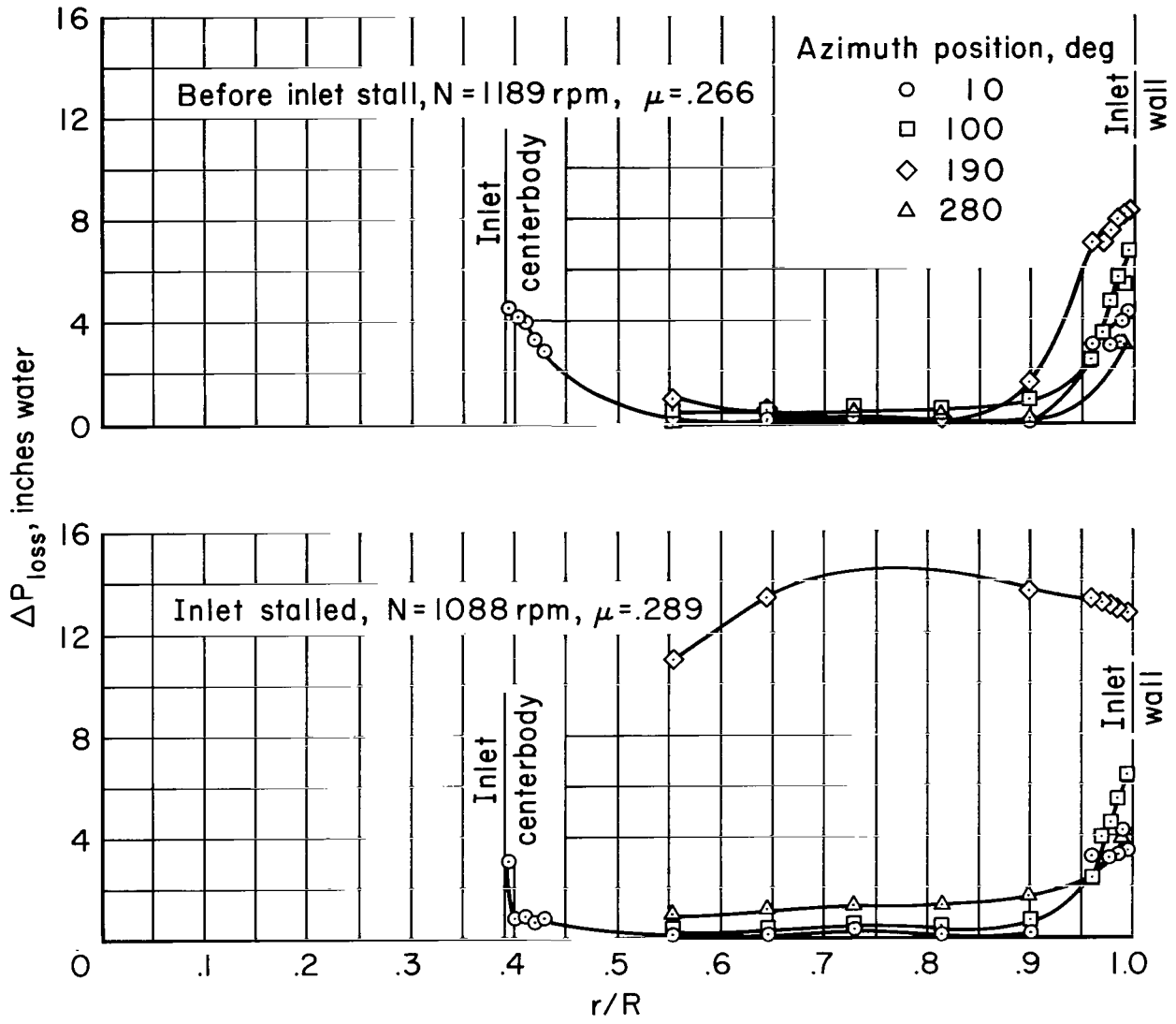

(b) $\alpha = 60^{\circ}$, $V_{\infty} = 51$ knots.

Figure 16.- Continued.

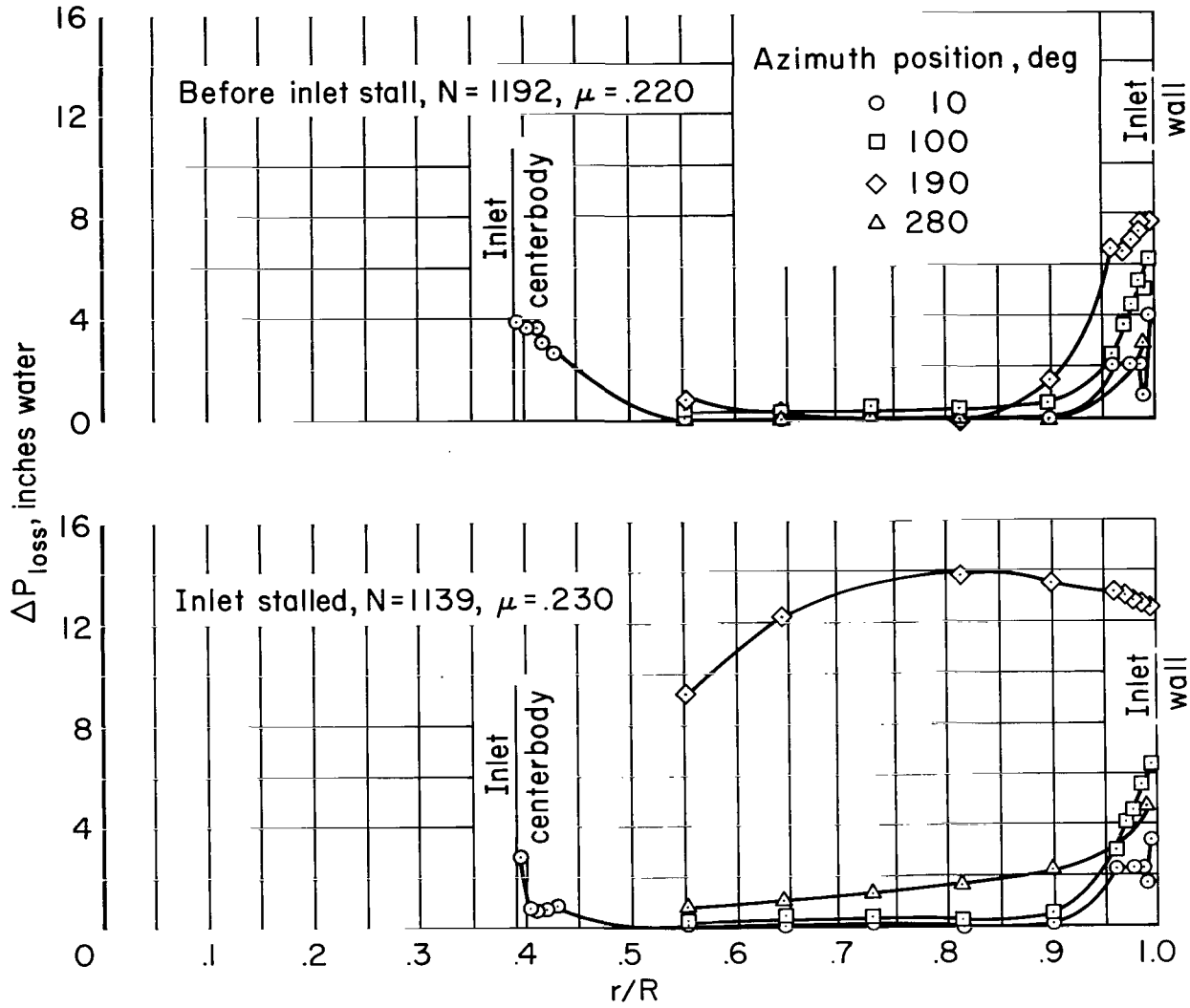

(c) $\alpha = 70^{\circ}$, $V_{\infty} = 42$ knots.

Figure 16.- Concluded.

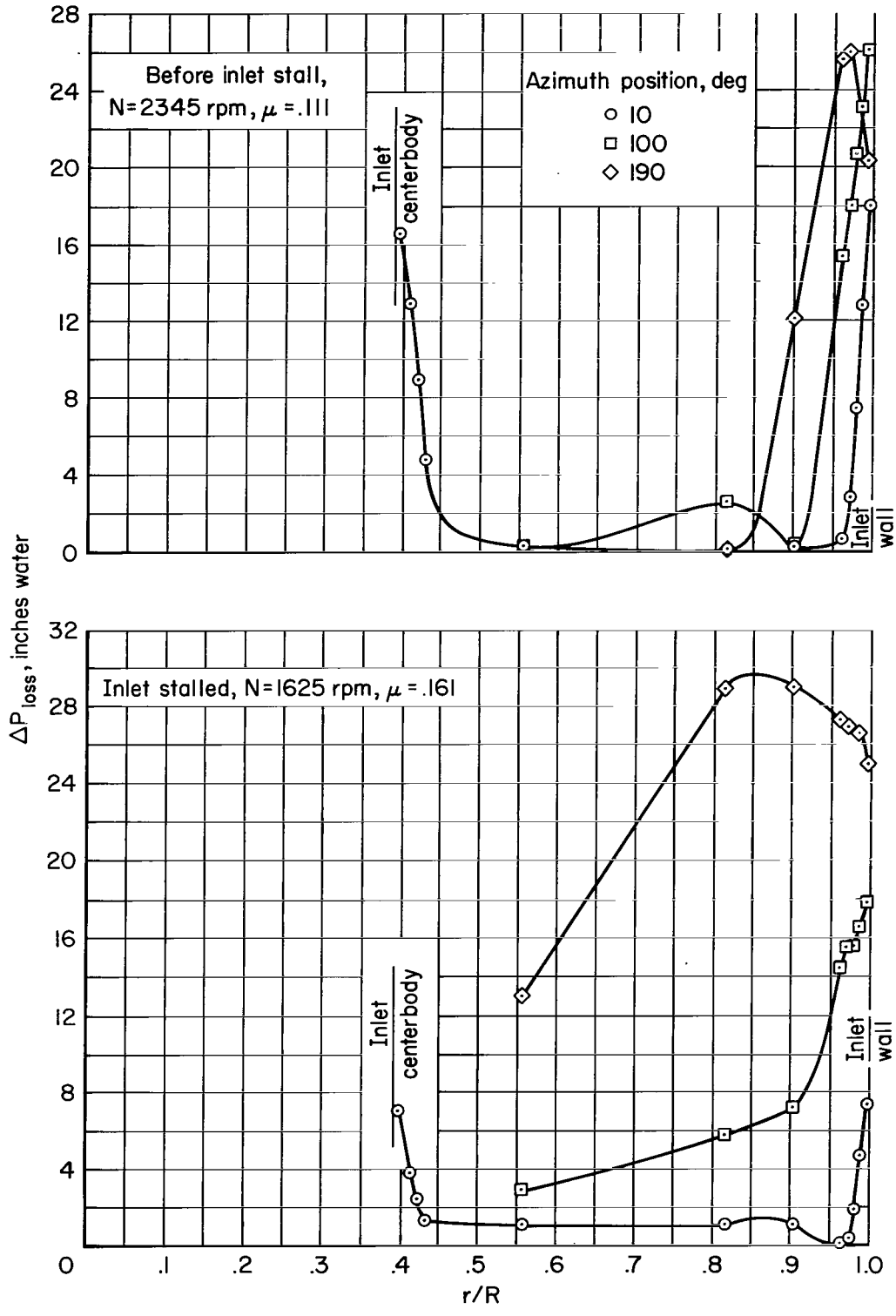

Figure 17.- Effect of duct inlet stall on the radial total pressure distribution in the inlet; $A_e/A_{e,s} = 1.0$, $\alpha = 80^\circ$, $V_\infty = 43$ knots.

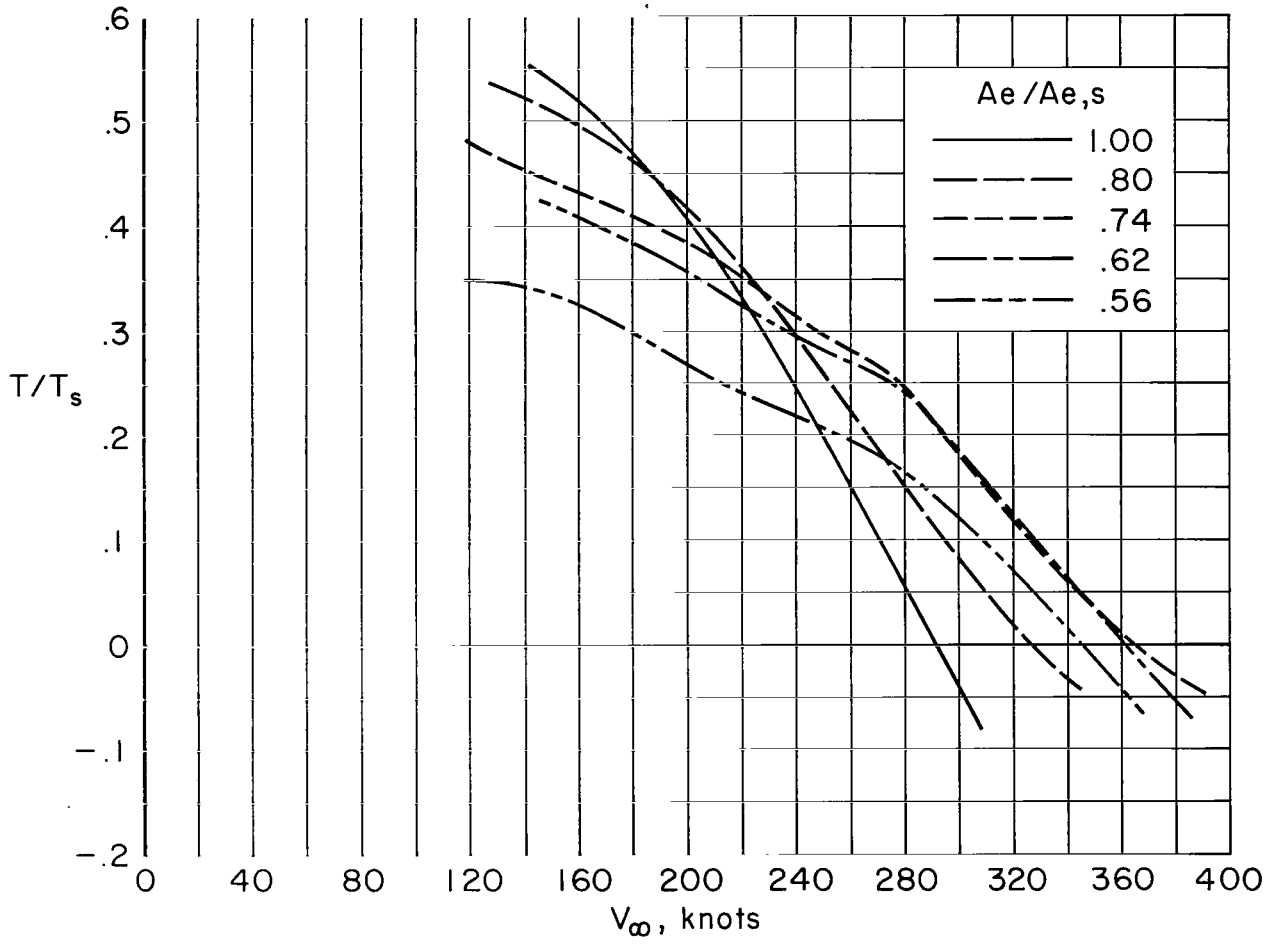

Figure 18.- Model performance showing the effect of duct exit area variation on net thrust with forward speed; $\alpha = 0^{\circ}$, N = 100 percent.

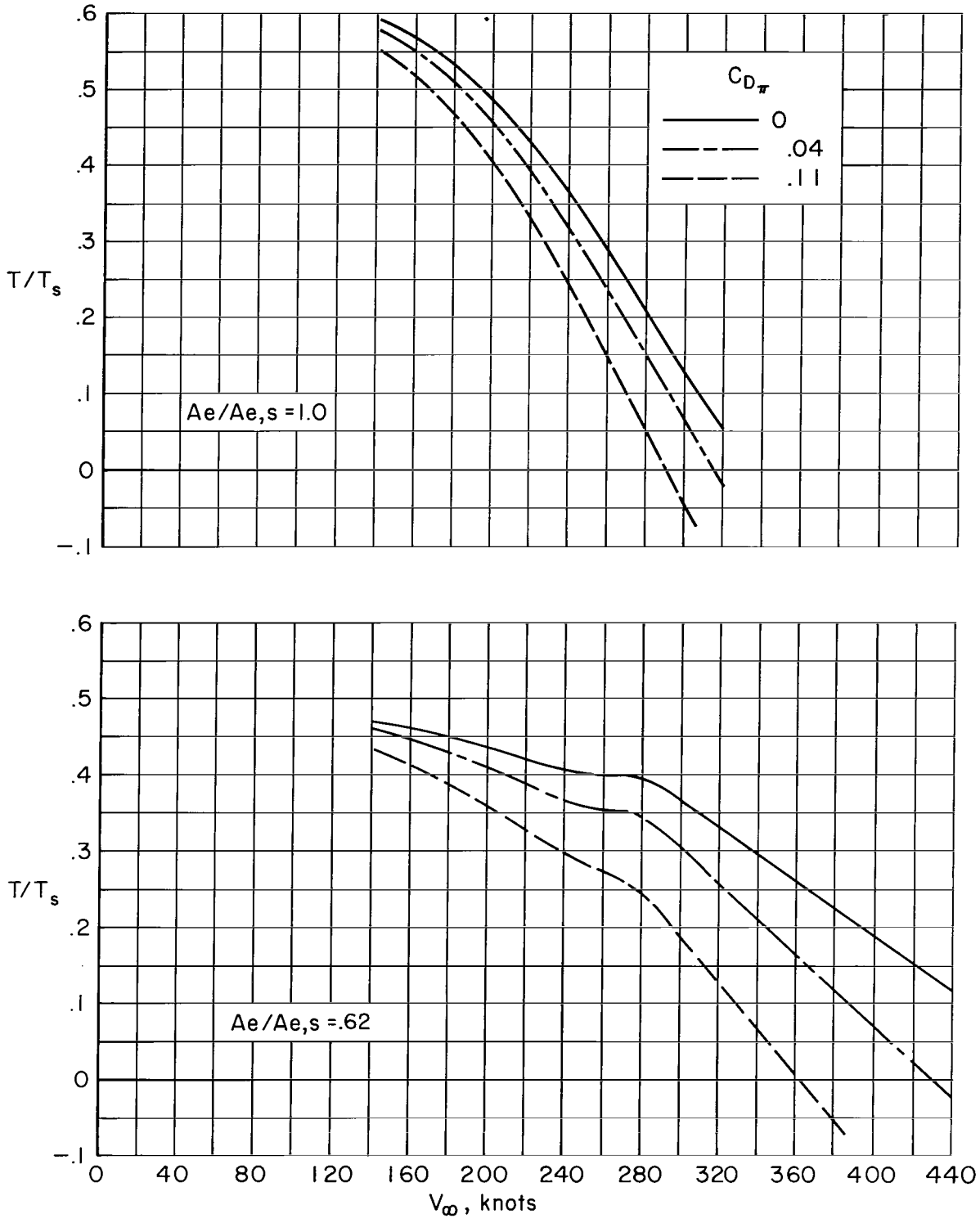

Figure 19.- Model performance showing the effect of external duct drag variation on net thrust with forward speed; $\alpha = 0^{o}$, N = 100 percent.

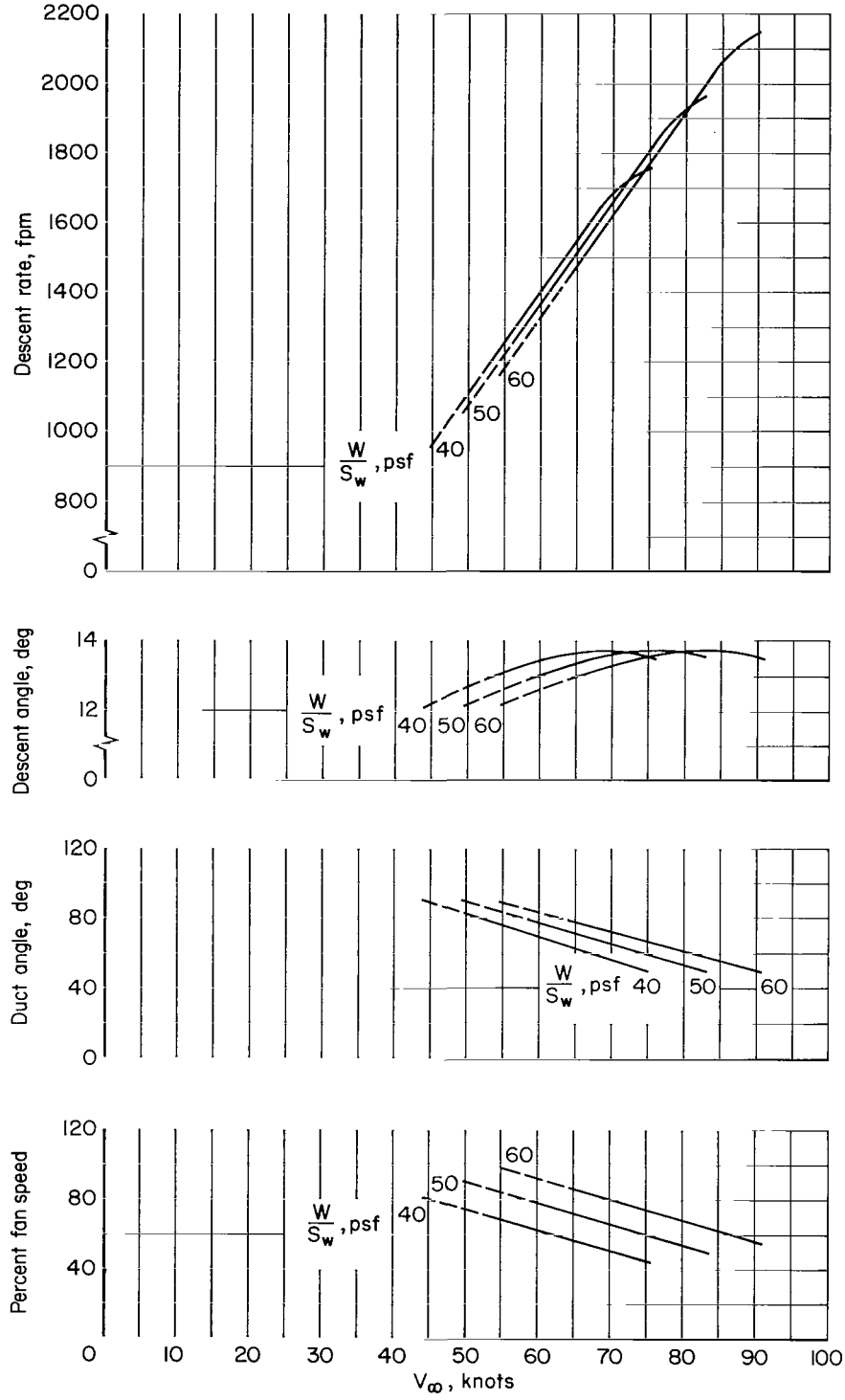

Figure 20.- Maximum descent conditions due to duct inlet stall for an airplane having two ducted lift-cruise fans; $A_e/A_{e,s} = 1.0$.

"The aeronautical and space activities of the United States shall be conducted so as to contribute . . . to the expansion of human knowledge of phenomena in the atmosphere and space. The Administration shall provide for the widest practicable and appropriate dissemination of information concerning its activities and the results thereof."

—NATIONAL AERONAUTICS AND SPACE ACT OF 1958

NASA SCIENTIFIC AND TECHNICAL PUBLICATIONS

TECHNICAL REPORTS: Scientific and technical information considered important, complete, and a lasting contribution to existing knowledge.

TECHNICAL NOTES: Information less broad in scope but nevertheless of importance as a contribution to existing knowledge.

TECHNICAL MEMORANDUMS: Information receiving limited distribution because of preliminary data, security classification, or other reasons.

CONTRACTOR REPORTS: Technical information generated in connection with a NASA contract or grant and released under NASA auspices.

TECHNICAL TRANSLATIONS: Information published in a foreign language considered to merit NASA distribution in English.

TECHNICAL REPRINTS: Information derived from NASA activities and initially published in the form of journal articles.

SPECIAL PUBLICATIONS: Information derived from or of value to NASA activities but not necessarily reporting the results of individual NASA-programmed scientific efforts. Publications include conference proceedings, monographs, data compilations, handbooks, sourcebooks, and special bibliographies.

Details on the availability of these publications may be obtained from:

SCIENTIFIC AND TECHNICAL INFORMATION DIVISION

NATIONAL AERONAUTICS AND SPACE ADMINISTRATION

Washington, D.C. 20546